MOLECULAR DYNAMICS STUDIES OF SURFACE DYNAMICS AND DYNAMIC HETEROGENEITY OF SUPERCOOLED METALLIC LIQUID

BY

YANQIN ZHAI

THESIS

Submitted in partial fulfillment of the requirements
for the degree of Master of Science in Nuclear, Plasma, and Radiological Engineering
in the Graduate College of the
University of Illinois at Urbana-Champaign, 2019

Urbana, Illinois

Master's Committee:

Professor Yang Zhang
Professor Jean Paul Allain

Abstract

Glasses play a significant roll in both modern manufacturing industry and scientific researches. However, the physical nature of glass, especially the unique issues on its surfaces, has remained unsolved for decades. In this work, we performed MD simulations on $Zr_{50}Cu_{50}$ supercooled metallic liquid in the bulk, near the free surfaces and the constrained surfaces at a target temperature of 900 K. The goal is to unveil the mechanism of enhanced mobility near the free surface. We examined the atomic motions by decomposing them into in-plane motions parallel to the interface and out-of-plane motions perpendicular to the interface. We found that the in-plane dynamics near the free surface is faster than the bulk, and surprisingly, the local structure near the free surface can be even more compact. Besides, the investigation on the exchange rate of atoms shows that the out-of-plane dynamics on the free surface was almost the same or even weaker than that in the bulk. The mean square displacement and the velocity autocorrelation function indicate an earlier termination of the cage effect and larger atomic arrangements near the free surface, which attenuates the phonons with higher energy and shifts the phonon density of states towards lower energy domain. In contrast, when the vacuum space is filled with pinned atoms, the mobility near the interface decreases to zero rapidly. These observations suggest that the enhanced dynamics near the free surface does not originate from larger free volumes, or, the atoms occasionally extracting themselves from the bulk and moving rapidly on the free surface. Instead, with missing coordination atoms in the vacuum space, the in-plane friction induced on those atoms on the free surface is halved, which finally strengthens the in-plane collective motions on the free surface.

Furthermore, we examined the temperature-dependence of dynamics and dynamic heterogeneity of $Zr_{50}Cu_{50}$ supercooled metallic liquid near the free surface. Dynamic heterogeneity can be displayed by the dynamic correlation length directly. RFOT theory proposed that the enhanced dynamics near the free surface is induced by the decreased dynamic correlation length. Here, the out-of-plane dynamic correlation length extracted from fitting the mobility gradient near the free surface shows little temperature dependence, which demonstrates the unique behavior of the outmost atomic layer on the free surface. However, the in-plane dynamic correlation length characterized by 2-dimensional $\alpha_{2,\max}$ was found to be larger on the free

surface than in the bulk. Considering the enhanced in-plane dynamics, we realize that the assumption made by RFOT theory that the dynamic rearranging region is hemispherical near the free surface is oversimplified. Instead, we propose that the dynamic rearranging region is distorted from 3-dimension to 2-dimension from the bulk to the free surface, which results in the counter-intuitive simultaneous enhancement of both dynamics and dynamic heterogeneity on the free surface.

To my father, mother, and Hanyu.

Acknowledgments

The author sincerely appreciates Professor Yang Zhang for his continuous and insightful guidance, which is critical and indispensable for this work. The author also sincerely appreciates Professor Jean Paul Allain for his taking valuable time to review this work and providing meaningful comments. The author appreciates the assistance from all of the group members in Z-Lab, especially Zhikun Cai, Nathan Walter, Zhixia Li, and Long Zhou, for inspirational discussions. The author appreciates the University of Illinois at Urbana-Champaign and the Department of Nuclear, Plasma, and Radiological Engineering and Beckman Institute for Advanced Science and Technology in the University of Illinois at Urbana-Champaign for the valuable resources they provided. The author appreciates the Illinois Campus Cluster Program for providing computing resources.

Table of Contents

List of Figures

List of Abbreviations

BMG	Bulk Metallic Glass.
DSC	Differential Scanning Calorimetry.
ECNLE	Elastically Collective Nonlinear Langevin Equation.
LAMMPS	Large-scale Atomic/Molecular Massively Parallel Simulator.
MCT	Mode-Coupling Theory.
MD	Molecular Dynamics.
RDF	Radial Distribution Function.
RFOT	Random First-Order Transition.
SNR	Signal to Noise Ratio.
VMD	Visual Molecular Dynamics.

List of Symbols

c_p	Isobaric Heat Capacity.
D	Diffusion Coefficient.
k_B	Boltzmann Constant.
P_c	Critical Pressure.
T_A	Arrhenius Crossover Temperature.
T_C	Mode-Coupling Transition Temperature.
T_D	Debye Temperature.
T_g	Glass Transition Temperature.
T_m	Melting Temperature.
T_v	Vaporization Temperature.
α	Variational Parameter.
α_p	Thermal Expansion Coefficient.
η	Shear Viscosity.
τ_α	Structural Relaxation Time.

Chapter 1

Introduction

1.1 Supercooled Liquids and Glasses

The three most common states of matter are gas, liquid, and solid. Even though modern physics classifies liquids and solids as condensed matter [2], which differ from gases, Van der Waals pointed out there is no qualitative difference between liquids and gases [3]. Both liquids and gases are the random disordered arrangement of particles and the only differences between liquids and gases are the packing ratio and the dynamics. With the temperature decreasing, the dynamics of particles in the gas becomes sluggish, while the packing ratio increases. Finally, as the temperature reaches the vaporization point T_v, a phase transition will bring the gas to the corresponding liquid with heat released below the critical pressure P_c while the gas will evolve continuously into liquid above P_c.

The transitions between the liquid state and the solid state are much more complicated. Figure 1.1 shows the temperature dependence of volume or enthalpy of liquids at constant pressure. Two typical transitions from liquids to solids are marked in the figure when temperature drops, which are the crystallization and the glass transition.

When the cooling rate is comparatively low, the rearrangements of particles in liquids happen and the system evolves into an ordered solid state to lower the free energy. This phenomenon is called the crystallization, and the temperature for the crystallization to happen is called the melting point T_m. Crystallization is a first-order thermodynamic phase transition, indicating that latent heat will be released. The vertical part of the blue line in Figure 1.1 marks this process.

However, if the system contains insufficient crystal nucleus or is under little perturbation, the crystallization can be avoided [4]. In this case, the system, corresponding to the region between the spinodal curve and the binodal curve in a phase diagram [5], is called supercooled liquids. Since supercooled liquids are thermodynamically unstable, perturbations such as stir or vibration can induce crystallization. The release of latent heat and the rearrangement of particles during the crystallization will reduce the entropy of the system, thus, the entropy of a supercooled liquid is expected to be higher than the entropy of the

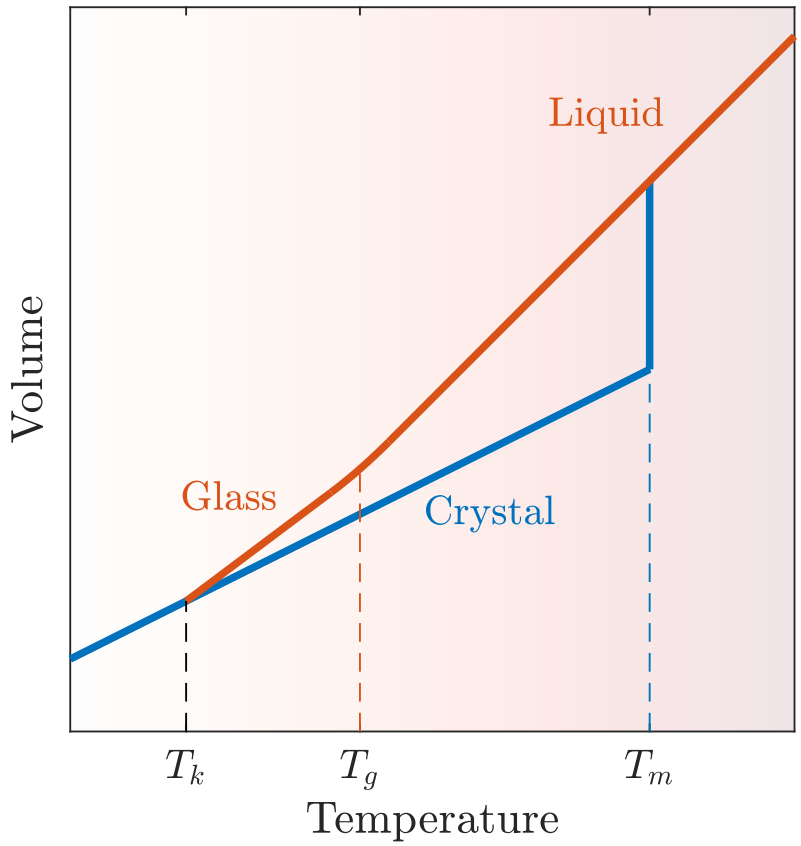

Figure 1.1: A demonstration of the temperature dependence of volume at constant pressure when liquids undergo crystallization and glass transition. T_m represents the melting point. T_g represents the glass transition points of glass-forming liquids. T_k represents the Kauzmann temperature.

corresponding crystal at T_m. Typically, the specific heat of a liquid is larger than that of the corresponding stable crystal at the given temperature. Therefore, the entropy difference between a supercooled liquid and its corresponding stable crystal at the temperature T_0 can be calculated by the following equation

$$\Delta S = \Delta S_m - \int_{T_0}^{T_m} \frac{\Delta C_p}{T} dT \tag{1.1}$$

where ΔS_m and ΔC_p represent the difference of entropy and specific heat between the supercooled liquid and its corresponding stable crystal at and below T_m respectively. According to Boltzmann's formula of entropy [5]

$$S(N, V, E) = k_B \ln\Omega \tag{1.2}$$

where S is the entropy of the system, k_B is Boltzmann constant, and Ω is the number of accessible quantum states in the microcanonical ensemble, entropy will always be non-negative. In addition, with the temperature approaching zero, the entropy of crystal also goes to zero due to the unique state of the lowest energy. Therefore, if the entropy of a supercooled liquid is lower than the entropy of the corresponding stable crystal, it will finally become negative with the temperature decreasing. This paradox is called the entropy crisis [6, 7, 8], and the temperature from where the entropy of supercooled liquid is extrapolated to be lower than that of the corresponding stable crystal is defined as the Kauzmann temperature T_K [9, 10]. The mathematical form of T_K is given by

$$\Delta S_m = \int_{T_0}^{T_m} \frac{\Delta C_p}{T} dT \tag{1.3}$$

via letting $\Delta S = 0$ in Equation 1.1. This crisis is practically avoided by the glass transition.

The physical nature of the glass transition is a fascinating issue that has haunted scientists for decades until recent [11, 12]. With supercooled liquids cooled sufficiently fast, even though some of them will lose metastability and crystallize [13, 14], others will fall out of equilibrium and form a solid-like state, the relaxation time of which will eventually exceed the timescale accessible in the laboratory. This phenomenon is called the glass transition, and corresponding liquids are called glass-forming liquids [15, 16]. Since T_g is always higher than T_K, and the physical properties including specific heat become time-dependent below T_g with the system aging, the entropy crisis can be temporarily avoided.

Whether the glass transition contains an underlying phase transition or is just a dynamical trapping is still under debate. There are several remarkable features of the glass transition. First, the thermal expansion coefficient α_p and the specific heat c_p suddenly but continuously change at T_g, which also depends on the

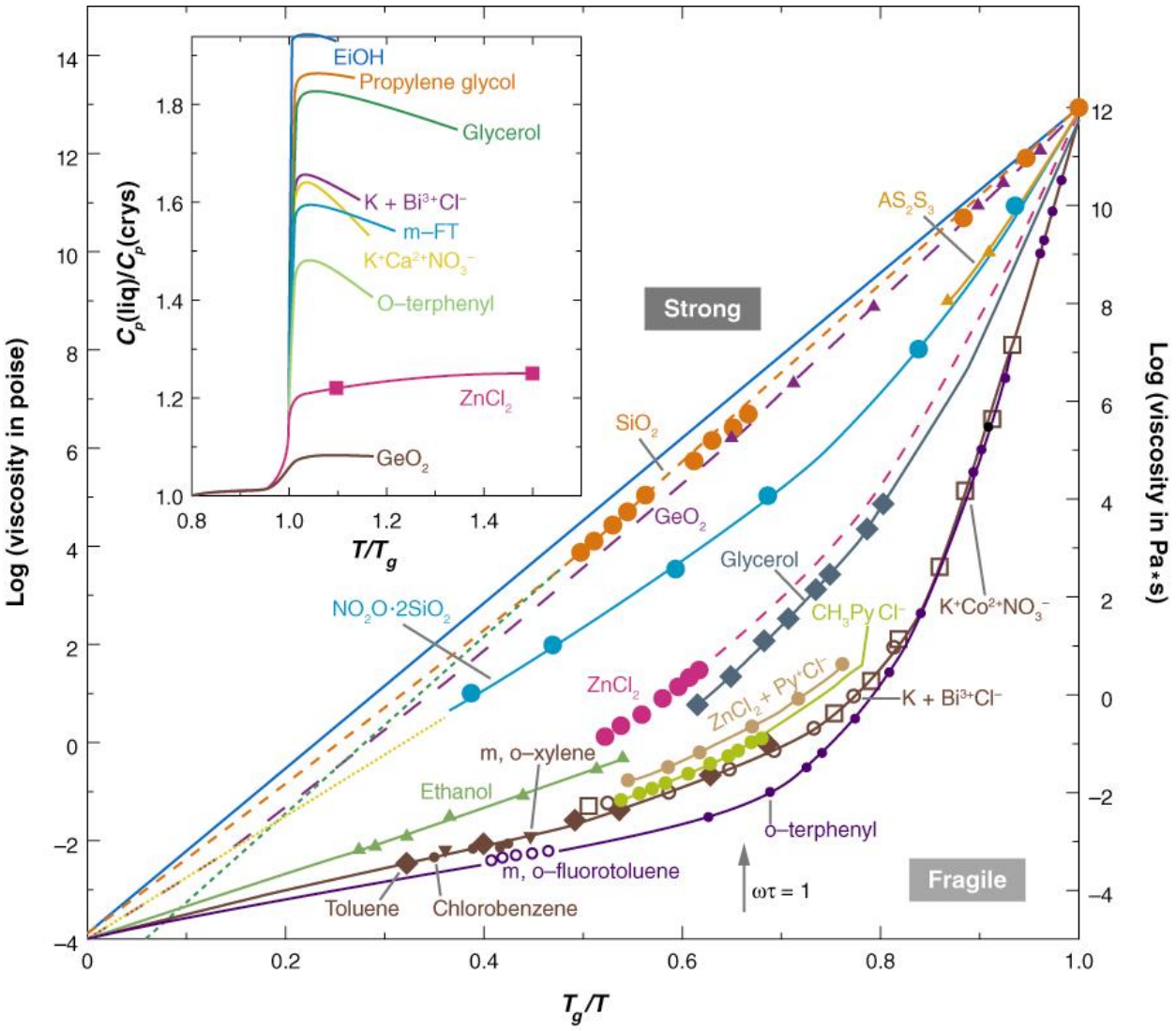

Lubchenko V, Wolynes PG. 2007.
Annu. Rev. Phys. Chem. 58:235–66

Figure 1.2: The logarithmic viscosities of various categories of strong and fragile liquids as a function of inverse temperature. The inner figure shows the ratio of specific heat of supercooled liquids to that of corresponding stable crystals near T_g. Figure taken from Reference [1].

thermal history of the system [6, 17, 18]. Based on this, the most frequently adopted definition of T_g is the intersection of the liquid and vitreous portions of the volume versus temperature curve, which is usually approximately equal to $2T_m/3$ and can be measured by differential scanning calorimetry (DSC) [6, 18]. The second feature of the glass transition is the accelerated increase of shear viscosity η when approaching T_g. Figure 1.2 shows viscosities of various categories of supercooled liquids as a function of inverse temperature, and the inner panel plots the abrupt change of specific heat at T_g. According to the relation of viscosity η on temperature near T_g, liquids can be classified as "strong" and "fragile" [11]. If the relation can be well described by the Arrhenius form

$$\eta = \eta_0 e^{E/k_B T} \tag{1.4}$$

where η_0 and E are independent of temperature and k_B is Boltzmann constant, the liquids will be classified as strong [19]. Otherwise, the liquids will be classified as fragile and the relation can sometimes be fitted by the Vogel-Tammann-Fulcher (VTF) equation [19, 20, 21, 22]

$$\eta = \eta_0 e^{B/(T-T_0)} \tag{1.5}$$

where η_0, B and T_0 are independent of temperature. Interestingly, some researches have shown that the temperature T_0 where the viscosity becomes divergent has a strong correlation with the Kauzmann temperature T_K [12]. Compared to strong liquids, fragile liquids exhibit a more obvious increase of viscosity over 2–4 orders of magnitude near T_g [23]. The sharp increase of the viscosity when the glass transition happens naturally leads to another definition of T_g—the temperature where the shear viscosity reaches 10^{13} poise [6]. The structural relaxation time τ_α shows a similar trend with the shear viscosity. From the perspective of viscosity or relaxation time, particles are dynamically trapped without noticeable structural rearrangement when the supercooled liquids undergo glass transition. Therefore, whether the glass transition is purely a dynamical slow-down process is still an open question for scientists.

As a summary, Figure 1.3 demonstrates the temperature regimes for liquid and glass physics. From high temperature to low temperature, T_v is the vaporization point and T_m is the melting point. Arrhenius crossover temperature T_A can sometimes be higher than T_m, and it represents a boundary of whether the transport of the liquids is predominated by collisions or energy landscape. Particles with higher mobility can move independently above T_A with phonon localized [24]. When the temperature is lower than T_A, the motions of the molecules start to be affected by the rugged energy landscape so that the cooperative motions predominate the transport and the dynamics become heterogeneous [25, 26]. T_g is the glass transition point and is always higher than the Kauzmann temperature T_K to practically avoid the entropy crisis. Below

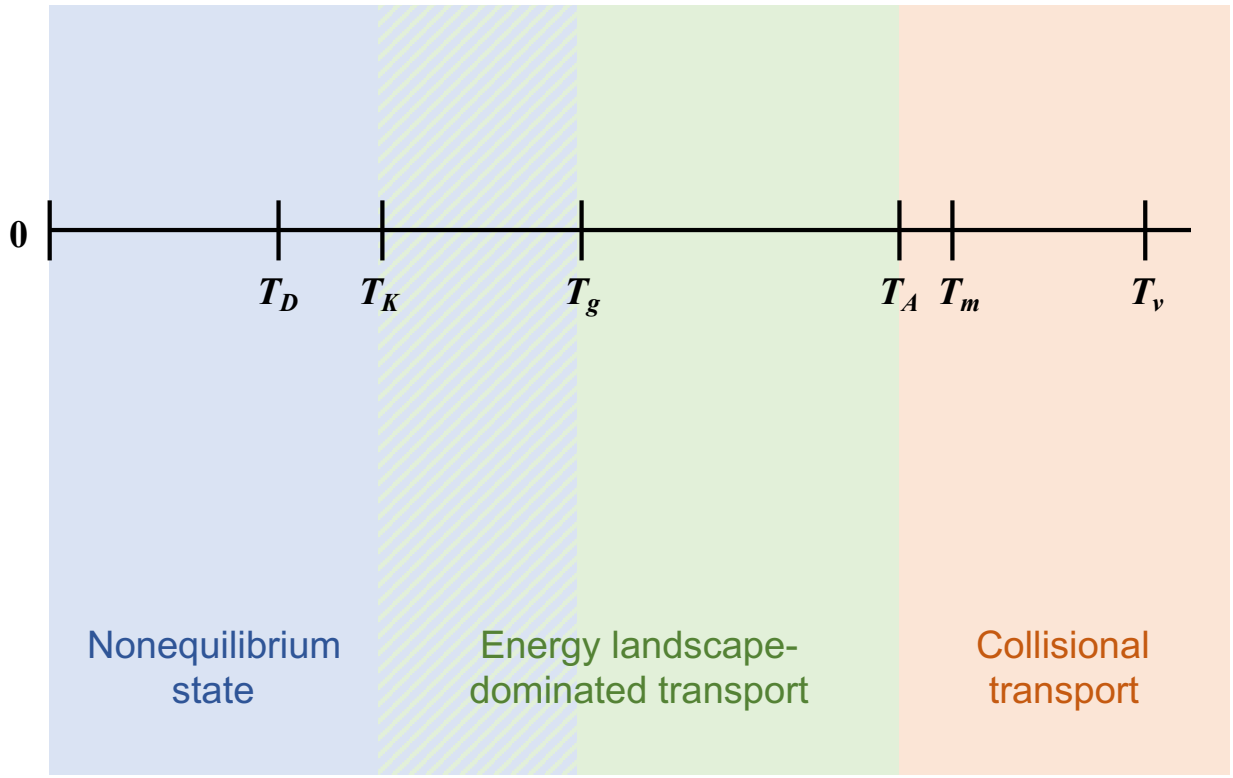

Figure 1.3: Temperature regimes for liquid and glass physics. T_v represents the vaporization temperature; T_m represents the melting temperature; T_A represents the Arrhenius crossover temperature from where the activated motions start to be predominant; T_g represents the glass transition temperature; T_K represents the Kauzmann temperature; T_D represents the Debye temperature. Figure adapted from Reference [1].

T_g, the typical structural relaxation time of the system exceeds the timescale accessible in the laboratory and the system falls out of equilibrium. Finally, T_D is the Debye temperature indicating the onset of the quantization of vibrational motions.

1.2 Enhanced Free Surface Mobility

One of the most intriguing issues remaining in the glasses is the enhanced free surface mobility and diffusion [27, 28, 29]. The mobility near the free surface of glasses has been observed to exceed that of the bulk by more than 6 orders of magnitude in polymer glasses [30, 31, 32, 33, 34], molecular glasses [35, 36, 37], or atomic glasses [38, 39, 40, 41, 42, 43, 44], and has been shown to be significantly larger than that of the corresponding melting crystal [45], from both experiments and simulations. More drastic relaxation due to the higher mobility on the free surface enables the glass to approach metastable states with lower free energy, which can be applied in developing ultrastable glasses by vapor deposition [46, 47, 48, 49, 50, 51].

Besides the enhanced mobility, there are several other associated intriguing phenomena near the free surface of glasses. As a consequence of the higher mobility, the local glass transition temperature near the free surface has been proved to be lower than that in the bulk [52]; the accelerated crystallization near the free surface has been observed in metallic glasses [42, 44]; the dynamic relaxation has been identified to be decoupled from the diffusion on the free surface of molecular glasses [53]; the Debye-Waller factor indicating the local mobility propensity [54, 55] near the free surface is significantly greater than that in the bulk [43]. Although plentiful phenomenological studies have been performed on the enhanced surface mobility from both experiments and simulations, it still lacks systematic and detailed research on the origin and impacts of this phenomenon, and the possible mechanism behind it is under drastic debate. The next section will cover the perspectives of theorists on this unsolved problem.

1.3 Theoretical Perspectives

Many theories, such as the energy landscape perspective [56] and the mode-coupling theory (MCT) [45], have been put forward to unveil the mysteries of the glass transition. Although these viewpoints have some weaknesses, they still provide insightful and comprehensive perspectives on the glass transition.

Energy landscape theory was put forward by Goldstein [56] in 1969 and has been adopted to describe the structure and dynamics of protein folding [57, 58, 59, 60, 61, 62, 63], the dynamics of supercooled liquids [64, 65, 66], and the mechanical properties of glasses [67, 68]. In detail, the potential energy of the system $\Phi(\boldsymbol{r}_1, \boldsymbol{r}_2, ..., \boldsymbol{r}_N)$ is determined by a set of generalized coordinates $\boldsymbol{r}_i$ of each particle, where N

represents the amount of the particles. The multidimensional potential energy surface versus the degree of freedom of the system constitutes the energy landscape. In the perspective of the energy landscape, the Arrhenius behavior of relaxation and transport properties of liquids at high temperature originates from the sufficient kinetic energy which endows ergodicity to the system. As temperature approaches T_A, the kinetic energy will no longer be adequate to support the system to surmount all of the energy barriers. Therefore, supercooled liquids will be trapped in local energy minima and the activation energy becomes temperature-dependent which induces a super-Arrhenius behavior of relaxation and transport properties [64]. Also, the energy landscape perspective explains the strong-fragile behavior of glass-forming liquids by the topographic distinction of the landscape, that is, the energy landscape of strong liquids consists of a single megabasin while the energy landscape of fragile liquids includes multiple well-separated megabasins [6]. Although the energy landscape provides a vivid picture to envision relaxation and transport within supercooled liquids and glasses, it is hard to be described with a strict and appropriate mathematical expression, to which, the mode-coupling theory (MCT) offers complementary viewpoints.

MCT regards the dynamic slow-down as a consequence of a feedback mechanism that transport diffusion contributes to the shear-stress relaxation and inversely relates to the viscosity which is proportional to the shear-stress relaxation time [6, 45]. MCT predicts a divergence of transport properties at temperature T_C where the kinetic arrest happens [69, 70]. However, as one found that $T_C > T_g$, a paradox appears, that the kinetic arrest predicted by MCT will advert when the system is still ergodic [71]. Although subsequent modification introduced additional relaxation to explain the paradox [72], there still exists other failures of MCT such as the inaccurate prediction on the non-Gaussian parameter

$$\alpha_2(t) = \frac{3\langle \boldsymbol{r}^4(t)\rangle}{5\langle \boldsymbol{r}^2(t)\rangle^2} - 1 \tag{1.6}$$

where

$$\langle \boldsymbol{r}^2(t)\rangle = \langle |\boldsymbol{r}(t) - \boldsymbol{r}(0)|^2\rangle \tag{1.7}$$

is the mean square displacement [71]. Thus, theorists are still complementing current theories or developing new theories to describe the glass transition self-consistently.

Random first-order transition (RFOT) theory proposed by Dr. Peter Wolynes [1, 15, 73, 74] provides another insightful thought to deal with the glass transition. RFOT theory first adopted the density functional form to describe the free energy of the system as

$$F[\rho(\boldsymbol{r})] = k_B T \int d^3\boldsymbol{r}[\ln\rho(\boldsymbol{r}) - 1] + \frac{1}{2}\int\int d^3\boldsymbol{r} d^3\boldsymbol{r}'[\rho(\boldsymbol{r}) - \rho_0]c(\boldsymbol{r}, \boldsymbol{r}'; \rho_0)[\rho(\boldsymbol{r}') - \rho_0] + F_{\text{uni}} \tag{1.8}$$

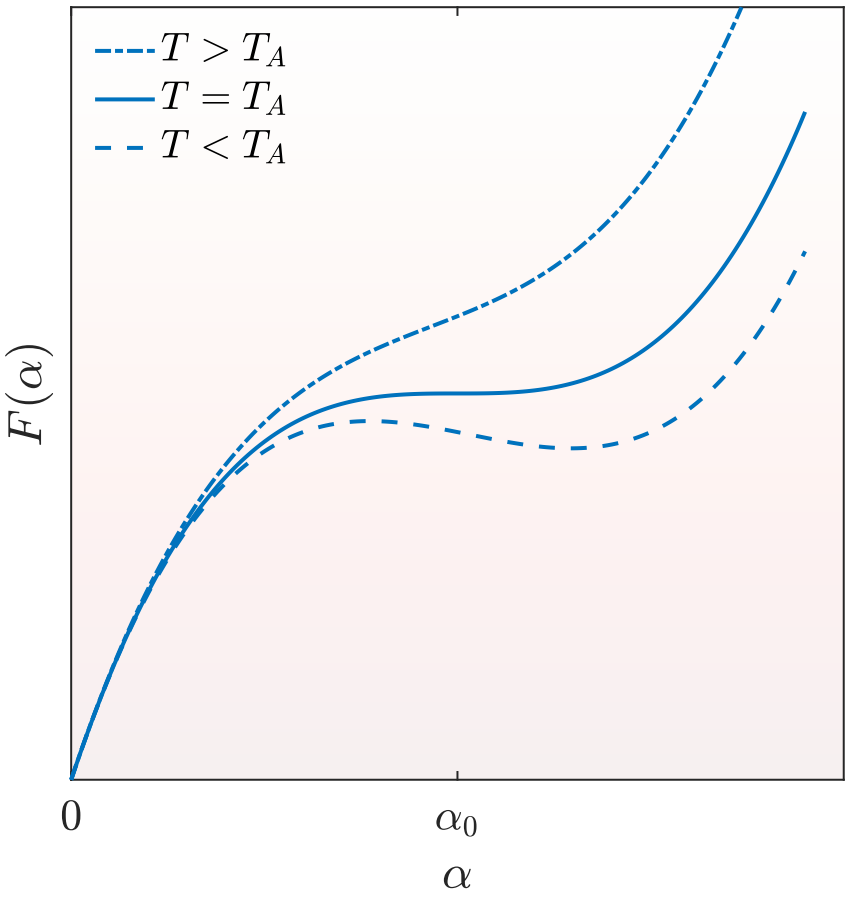

Figure 1.4: A demonstration of the appearance of the second minimum $\alpha = \alpha_0$ of the free energy $F(\alpha)$ at T_A. Figure adapted from Reference [1].

where k_B is Boltzmann constant, T represents temperature, $\rho(\boldsymbol{r})$ is the density distribution of the system, and F_{uni} is the free energy of the uniform liquid [75, 76]. The first term on the right-hand side of Equation 1.8 represents the entropy of ideal gas, while the second term represents the potential energy that takes only the lowest order of interaction between particles into consideration. RFOT theory employs a Gaussian form to describe the variational profile of density as

$$\rho(\boldsymbol{r}) = \sum_i (\frac{\alpha}{\pi})^{3/2} e^{-\alpha(\boldsymbol{r}-\boldsymbol{r}_i)^2} \tag{1.9}$$

where $\boldsymbol{r}_i$ represents the coordinates of particles in an aperiodic lattice, and α is the average lattice space [1, 77]. According to Equation 1.9, $\alpha = 0$ indicates a completely delocalized regime corresponding to uniform liquids, while $\alpha \neq 0$ indicates a localized regime where transient local quasiharmonic environment forms [1]. As a function of α, the free energy $F(\alpha)$ of a supercooled liquid always has a single minimum $\alpha = 0$ at sufficiently high temperature, nevertheless, as temperature decreases to T_A, a non-zero minimum $\alpha = \alpha_0$ emerges [74, 78] as Figure 1.4 shows, indicating the formation of metastable structures at T_A. The transition of the minimum from $\alpha = 0$ to $\alpha = \alpha_0$ resembles a first-order phase transition, explaining the "first-order" in the name of the theory. The transition is called random because "Although first order in α, it results in many random (infinite-lifetime) phases that are distinct both morphologically and spatially" [1]. A detailed discussion of the RFOT theory can be found in Reference [1] and therein.

Many important conclusions and predictions have been made by the RFOT theory. For example, it directly derives the VTF law via

$$F^{\ddagger} = \frac{\gamma^2}{4\Delta c_p (T - T_K)} \tag{1.10}$$

where $F^{\ddagger}$ is the most probable relaxation barrier [1], and it predicts the scale of dynamical heterogeneity length ξ as [15]

$$\xi^{\ddagger} \propto \frac{1}{(T - T_K)^{2/3}} \tag{1.11}$$

Those predictions can be directly compared with data obtained from experiments and computer simulations, and have been testified to have good agreement with observations.

The RFOT theory also provides an explanation for the enhanced dynamics near the free surface [79]. In their perspective, the activation energy near the free surface should be one half of that in the bulk. However, the neglect of coarse structures and static perturbations on the surface restrains the validity and feasibility of the theory.

Recently, some latest theories focusing on the glassy system have also proposed hypotheses on the mech-

anism of enhanced mobility near the free surface, including the elastically collective nonlinear Langevin equation (ECNLE) theory [80, 81] and the theory put forward by Dr. Simmons [82]. All of these theories predict an exponential increment of the mobility as a function of the depth to the free surface, or, the mobility gradient near the free surface obeys an exponential form. In the following content, We will demonstrate that this prediction aligns with our observations from MD simulations.

1.4 Workscope

Metallic glass, also known as amorphous metals, was first produced in 1960 [83]. Unlike common crystalline metal, the suddenly quenching process freezes the atoms and prevents them from crystallization, thus, it brings the system into a glassy state. The metallic glass was first made into stripes due to the limitation of the cooling rate [83, 84, 85]. Recent development enables the manufacture of large bulk metallic glasses (BMGs) [86, 87, 88, 89]. The thoroughly different properties of BMGs from conventional crystalline metals, such as higher tensile yield strengths and hardness, higher elastic strain limits, higher wear and corrosion resistance, lower thermal conductivity, and easier castability [90, 91, 92, 93], endow BMGs unique applications including nanoparticles, nanoimprint lithography, field electron emission devices, artificial bones, etc. [93, 94, 95, 96]

For our interests, the simple atomic constitution of metallic glasses with no intramolecular structure makes it a comparatively simple model to study the structural and dynamic properties of glasses. In our work, we employed $Zr_{50}Cu_{50}$ supercooled metallic liquid as a model and performed MD simulations to explore the structural and dynamic properties both in the bulk and near the interfaces. From the computation of normalized depth-dependent density, we found that the local density near the free surface is even greater than that in the bulk. Within this region, the mean square displacement and the velocity autocorrelation function identified an enhanced in-plane surface dynamics, which shifts the phonon density of states towards the lower energy domain. Further examination of out-of-plane motions showed that the out-of-plane dynamics were not enhanced. We, therefore, concluded that the enhanced dynamics near the free surface is introduced by the missing coordination atoms in the vacuum space which halve the friction, and thus, accelerate the in-plane dynamics within the outmost atomic layer. In addition, we also investigated temperature dependent dynamic heterogeneity from in-plane and out-of-plane dynamic correlation lengths characterized by mobility gradient and in-plane non-Gaussian parameter, respectively. It revealed the particularity of the outmost atomic layer, where the dynamics are strengthened and more heterogeneous. By modifying the assumption made by RFOT theory, we finally credited the mechanism of this phenomenon to the extension of the in-plane dynamic rearranging region as a consequence of the enhancement of in-plane mobility.

The thesis is divided into four chapters. The first chapter provides a background introduction. The second chapter will discuss the phenomenon and the mechanism of enhanced mobility near the free surface of the supercooled metallic liquid with simulation done at a certain temperature. The next chapter is going to investigate a counter-intuitive phenomenon that both the dynamics itself and dynamic heterogeneity are enhanced within the outmost atomic layer near the free surface which is contradictory with the prediction of existing theory. The final chapter, will summarize the findings in this thesis and outlook on the complementary work in the future.

Chapter 2

Study of Enhanced Dynamics on the Free Surface of Supercooled Metallic Liquid

In this chapter, we discuss our MD simulations on $Zr_{50}Cu_{50}$ supercooled liquid to study the structural and dynamic properties in the bulk, near the free surface and the constrained surface. The target temperature of the simulation in this chapter was set to 900 K between the reported T_g = 677 K and T_m = 1231 K [97]. The first section demonstrates the setup and detailed processes of our simulation. The second section successively enumerates introductions and calculations of various quantities to characterize the structures and dynamics in the system. Proper discussion follows the demonstration of each quantity. Finally, we glue pieces of evidence together and put forward our hypothesis of the mechanism of enhanced dynamics near the free surface. The last section summaries the discussion in this chapter and draw conclusion explicitly.

2.1 Method

We performed MD simulations on three $Zr_{50}Cu_{50}$ supercooled liquid systems with different configurations including (a) a bulk, (b) with two free surfaces, and (c) with two constrained surfaces as shown in Figure 2.1 respectively. For each system, 50000 zirconium atoms and 50000 coppers atoms were placed in cuboid boxes with periodic boundary conditions enforced in all three dimensions.

For the bulk system, the dimensions of the simulation box were initially set to $120.0 \times 120.0 \times 120.0$ Å^3. Enforced in the NPT ensemble, the system was equilibrated at 2000 K for 1 ns and quenched to the target temperature 900 K with a cooling rate of 10^{12} K/s. After equilibrated for 5 ns in the NPT ensemble, the system was carried out for 5 ns while the atomic number density was collected and averaged to be 0.0554 Å^{-3} which was adopted in the following simulations. According to the corrected density, the side length of the simulation box was reset to 121.75 Å, and all of the following simulations were carried out in NVT ensembles. The system was well equilibrated again at 900 K for 5 ns after the dimensions of the simulation box got adjusted, then was ready to generate trajectories.

For the system with two free surfaces, a cuboid simulation box with dimensions $212.4 \times 212.4 \times 40.0$ Å^3 was first created. The system was first equilibrated at 2000 K for 1 ns, then, quenched to 900 K with the

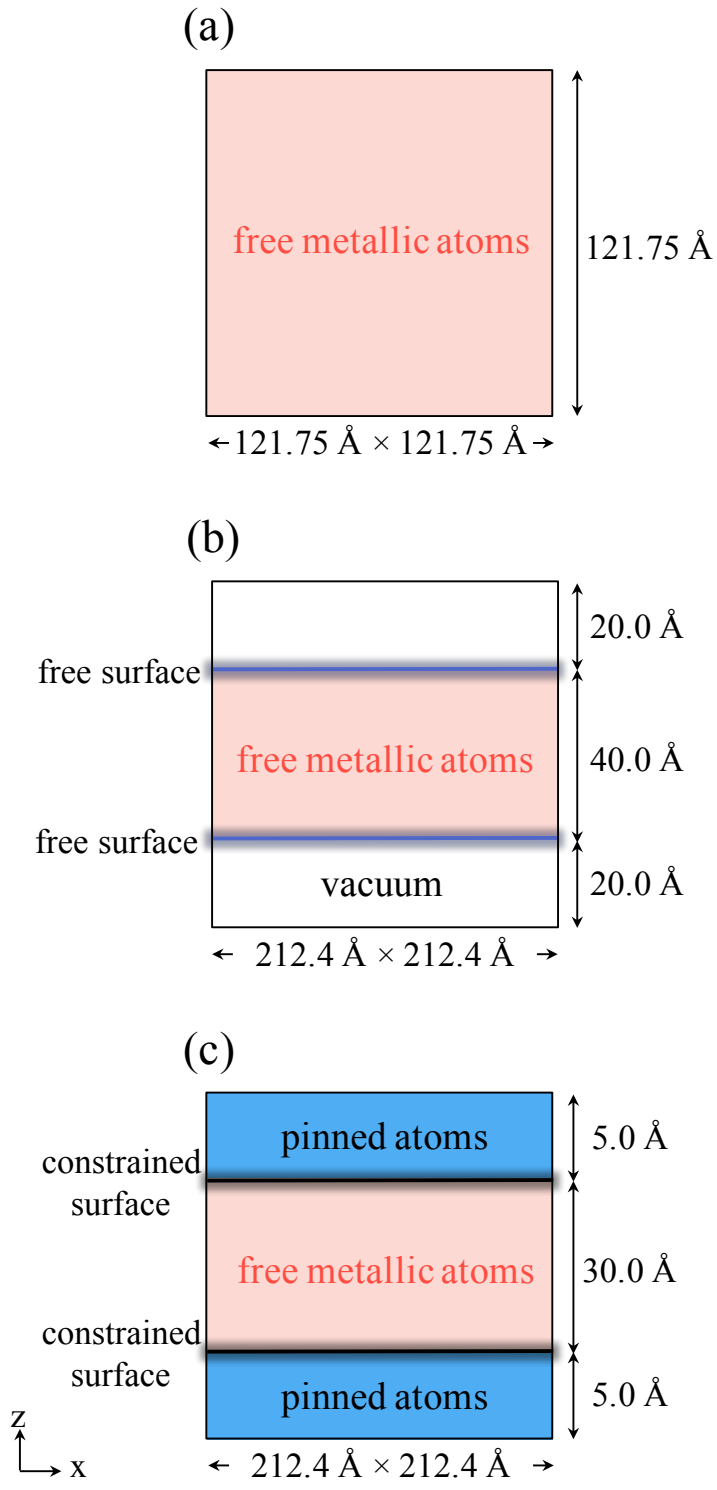

Figure 2.1: Schematic of the setup of simulation $Zr_{50}Cu_{50}$ supercooled liquid systems including (a) a bulk system, (b) a system with two free surfaces, and (c) a system with two constrained surfaces. Dimensions of the systems are marked out. The origins are placed on and the z-axes are set perpendicular to the surfaces.

same cooling rate. After the system had been well equilibrated for 5 ns, the simulation box was doubly enlarged in the z-direction, creating two free surfaces perpendicular to the z-axis and reserving two vacuum volumes to avoid the interaction from periodic images. Finally, the system was equilibrated for another 5 ns before ready to generate simulation trajectories.

For the system with constrained surfaces, a cuboid simulation box with dimensions $212.4 \times 212.4 \times 40.0$ Å^3 was first set up. The system was first equilibrated at 2000 K for 1 ns, and then quenched to 900 K with the same cooling rate. After the system had been well equilibrated for 5 ns, the atoms locating in the two regions within 5 Å to the boundary of the simulation box in the z-direction were pinned, so that two constrained surfaces were created as demonstrated in Figure 2.1(c). With the rest of the atoms between two constrained surfaces free to move, the system was well equilibrated for 5 ns, and finally, we started to collect trajectories for unfixed atoms.

For all of the three systems, the integration time step was set to 1 fs using the Verlet algorithm [98], and for each system, trajectories were dumped in two different ways—a short dense trajectory dumped every 1 fs for 10^5 frames and a long sparse trajectory dumped every 100 fs for 10^5 frames. This dumping strategy brought convenience for computing dynamical properties both in a short time scale such as the velocity autocorrelation function or in a long time scale such as the mean square displacement. All of the simulations were carried out using Large-scale Atomic/Molecular Massively Parallel Simulator (LAMMPS) [99]. Interactions between zirconium and copper atoms were described by a binary EAM potential [100]. The temperature and the pressure were controlled by the Nosé-Hoover thermostat and barostat respectively [101, 102, 103]. The trajectories were analyzed using LiquidLib [104], a C++ based package for post-processing simulation trajectories developed by our group. Three-dimensional visualizations were conducted using Visual Molecular Dynamics (VMD) [105].

The target temperature of our simulations is 900 K which largely exceeds the glass transition temperature of the system (677 K). Besides, we well equilibrated the systems for at least 5 ns before collecting trajectories. Therefore, the ergodicity of our simulation can be guaranteed. In the calculation of each quantity, we took an ensemble average of at least 50000 frames, which was supposed to well represent the real ensemble. Therefore, the uncertainty, which only originates from the round-off error of the computation device and the error that we assume our trajectory can well represent the real ensemble, is supposed to be negligible in our calculations.

2.2 Normalized Depth-Dependent Density

For the systems with free surfaces or constrained surfaces, we first examined the effects of the surfaces on local structures. In an isotropic system, the structure is usually described by radial distribution function (RDF) [106]

$$g(r) = \frac{1}{\rho}\langle\sum_{l\neq l'}\delta(r - |\boldsymbol{r}_l - \boldsymbol{r}_{l'}|)\rangle \tag{2.1}$$

where $g(r)$ is RDF, ρ is the average atomic number density of the bulk system, $\boldsymbol{r}_l$ is the coordinates of the l-th particle, $\delta(x)$ is the Dirac delta function, and $\langle\cdot\rangle$ takes the average over the corresponding ensemble. RDF provides a description of the average structure and the inter-particle interactions in the isotropic system and can be directly measured by scattering experiments. Therefore, RDF is insightful and significant in structural characterization.

In an anisotropic system, however, RDF no longer works. Instead, we adopted a normalized depth-dependent density function (shown in Figure 2.2) calculated by

$$\rho(z) = \frac{1}{\rho_0}\langle\sum_{l\neq l'}\delta(|z_l - z_{l'}|)\rangle \tag{2.2}$$

to characterize the structures of the systems with long-range broken symmetry. In Equation 2.2, $\rho(z)$ represents the normalized depth-dependent density, ρ_0 represents the density of the bulk system, z_l is the z-component of the l-th atom's coordinates, and $\langle\cdot\rangle$ takes the average over the corresponding ensemble. Comparing Equation 2.1 with Equation 2.2, RDF describes the surrounding radial density fluctuation by regarding each atom as the center while $\rho(z)$ provides information about layered density fluctuation from bulk to the surface. Thus, $\rho(z)$ can be analogous to and regarded as a substitution of $g(r)$ in anisotropic systems, which provides the same category of structural and interactional information.

During practical calculations, the summation of δ functions is usually implemented by a binning strategy, that is, the range of $z \in (z_0, z_N)$ is evenly divided into N continuous bins $\{(z_0, z_1), (z_1, z_2), \cdots, (z_{N-1}, z_N)\}$, and each atom is classified into the corresponding bin according to its z-component of the coordinates. Finally, the number of atoms classified into bin (z_i, z_{i+1}) is adopted to represent the local density at $z = (z_i + z_{i+1})/2$ where $i = 0, 1, \cdots, N-1$. To be specific,

$$\rho(\frac{z_i + z_{i+1}}{2}) \approx \frac{\langle N_i\rangle}{\rho V_i} \tag{2.3}$$

where N_i represents the number of atoms in the i-th bin, V_i represents the volume of the i-th bin, ρ is the atomic number density of the bulk system, and $\langle\cdot\rangle$ takes the average over the corresponding ensemble. Since

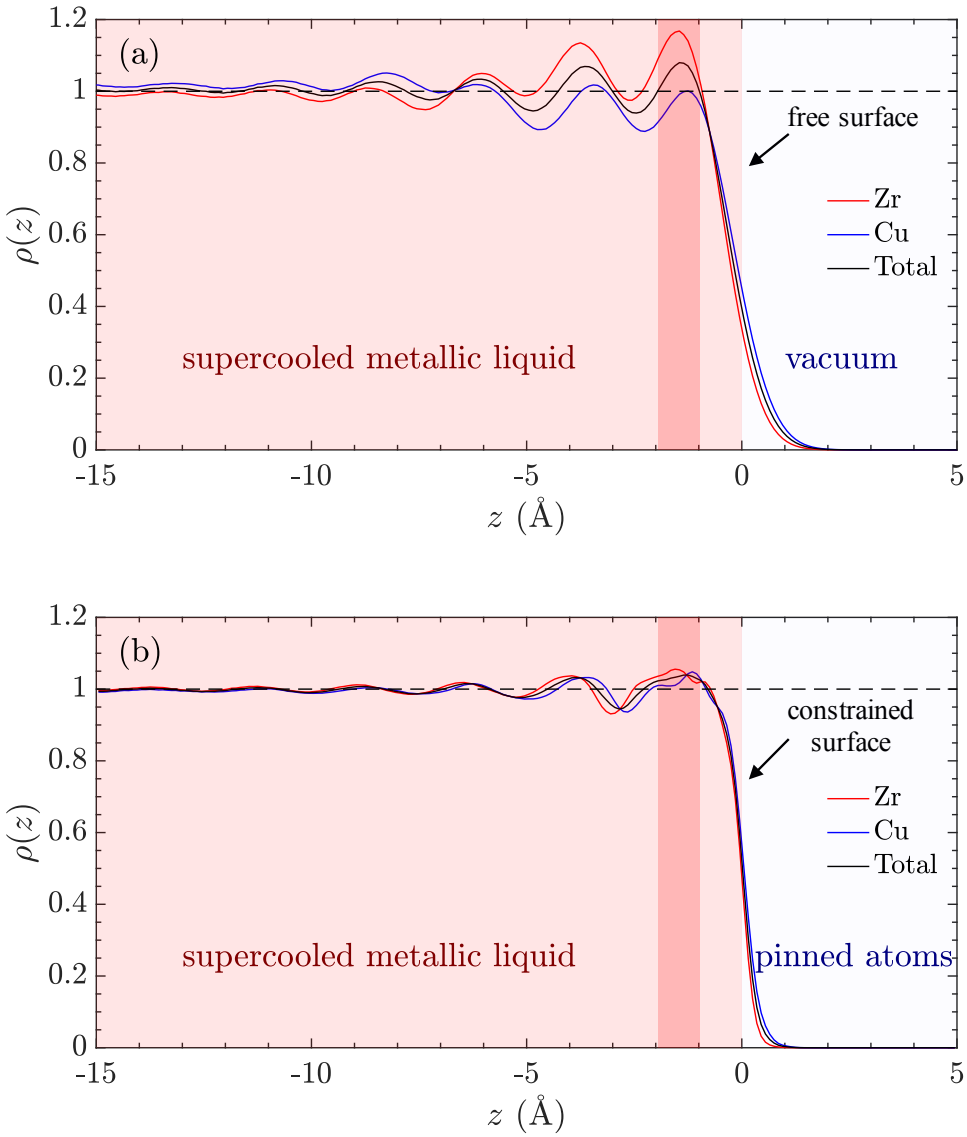

Figure 2.2: The normalized depth-dependent density of $Zr_{50}Cu_{50}$ supercooled metallic liquid systems (a) with free surfaces and (b) with constrained surfaces at 900 K. The origins are set on the surface and z represents the depth to the surfaces. The normalization is performed by dividing the local atomic number density of the systems with surfaces by the value of the bulk system, thus, the normalized depth-dependent density of the bulk system is 1 and indicated by the black dash line. The light pink regions represent the supercooled metallic liquid where the atoms are free to move. The light cyan regions represent the vacuum space in figure (a) and pinned atoms in figure (b). The boundaries between the two regions located at $z = 0$ represent the free surfaces in figure (a) and the constrained surfaces in figure (b). The deep pink stripes covering around $z = -2$ to $z = -1$ indicate the regions where the total normalized local density is larger than 1.

$\rho(z)$ becomes discrete after the binning strategy adopted, the number of bins N is a critical parameter which significantly affects the resolution and the signal to noise ratio (SNR) of $\rho(z)$. If the distribution of the bins is excessively sparse, the fine structural fluctuation in the system will be omitted, which might reduce the resolution of $\rho(z)$. On the other hand, if the distribution of the bins is unnecessarily dense, the peaks contributed by δ functions will become towering and noisy, and cover up the average structural information of $\rho(z)$. During our calculations, the bins were evenly distributed with a width of 0.1 Å, which has been proved by the fact to hold a reasonable resolution and be able to reflect local structures.

Figure 2.2 shows the normalized depth-dependent density of the $Zr_{50}Cu_{50}$ supercooled metallic liquid (a) with free surfaces and (b) with constrained surfaces at 900K. The light pink regions with negative z represent the inner metallic atoms with free mobility. The light cyan regions with positive z represent the vacuum volume in figure (a) and represent the pinned atoms in figure (b), respectively. Therefore, both the free surfaces and the constrained surfaces are located at $z = 0$. The red, blue and black solid lines represent the $\rho(z)$ of zirconium, copper, and totality respectively, and the $\rho(z)$ of the bulk system is indicated by the black dash lines located at $\rho(z) = 1$ as a reference.

A periodic density fluctuation near the free surfaces can be clearly observed in Figure 2.2(a). Sine-shaped oscillation of $\rho(z)$ indicates the existence of an ordered layer structure. The closer to the free surfaces, the more violent the oscillation is, which means that the structure near the free surfaces is more ordered than the structure in the bulk. Surface crystallization has been observed in metallic glasses either by experiments [42] or simulations [107]. Whether crystallization is induced by the enhanced free surface mobility is under discussion [42]. However, our observation contradicts this hypothesis, and details will be discussed in the following content. Another interesting phenomenon is that near the free surfaces, the density of zirconium is higher while the density of copper is lower than those in the bulk. Therefore, zirconium tends to accumulate near the free surfaces while copper prefers a bigger coordination number. This can be explained by that the attractive interaction between copper is stronger than that between zirconium [100]. When the free surfaces are introduced, copper prefers to stay inside the bulk with fully coordinated while leaving zirconium to the surfaces with broken coordination. As a consequence, the free energy is reduced and the whole system is more thermodynamically stable.

Oscillation of density profile was also observed near the constrained surfaces but is not as strong as that near the free surfaces. The observation of ordered layer structures near either the free surfaces or the constrained surfaces refutes the possible origin from enhanced mobility. Here, we argue that the formation of layer structure is due to the symmetry-broken interaction near the surfaces. When the surface exists, the broken symmetry of the structure on the surface results in imbalanced interaction, which affects the structure

itself in reverse. In addition, there is no obvious preference of a certain type of element to accumulate near the constrained surfaces because of the same number of coordination in the bulk or on the interface, which differs from the situation on the free surfaces.

2.3 Mean Square Displacement

Besides static structural properties, we further examined dynamic properties including mean square displacement, velocity autocorrelation function, phonon density of states, and diffusion coefficient for all of the three systems. For the systems with surfaces, we evenly divided the systems into multiple layers perpendicular to the z-direction, so the atoms in each layer are assumed to have the same dynamics because of the approximately same depth to the surfaces in the z-direction and the enforced periodic boundary conditions in the x- and the y-directions. All of the dynamic properties mentioned below were calculated in 2-dimension, and therefore, reflect the in-plane dynamics as functions of depth to the surfaces. Resembling the binning strategy, the width of the layers should also be determined carefully. Over-widely layering might cause a poor resolution in the z-direction and the assumption of the unified dynamics in the same layer might no longer be valid. On the other hand, excessively narrowly layering might induce noisy due to insufficient statistics with a limited number of atoms in each layer. In our simulations, we adopted a layer width of 1.0 Å which is smaller than the Van der Waals radii of the copper atom (1.40 Å) and zirconium atom (2.30 Å) in order to guarantee a detailed resolution. Besides the dilemma of layering, the definition of which atoms belonging to a certain layer was also tricky. In our simulation, the atom was designated into a specific layer if the center of that atom was in the layer both at t_0 (initial time) and t, that is, even if the atom had moved out of the layer and moved in again, we still designated it into that layer. The advantage of this treatment is the economy of computation. In addition, considering our neglect of out-of-plane motions and no diffusion on the surfaces due to periodic boundary conditions, this treatment should be quantitively acceptable and was adopted in all of the following computations. For the bulk system, the dynamic quantities were calculated in 3-dimension and scaled by 2/3 to be compatible with 2-dimensional versions. Detail explanation and analysis of each property are illustrated in the following content.

Mean square displacement describes the deviation of the positions of particles over time respect to their original positions and is computed by

$$\langle r^2(t)\rangle = \frac{1}{N}\langle\sum_{l=1}^{N}|\boldsymbol{r}_l(t)-\boldsymbol{r}_l(0)|^2\rangle \tag{2.4}$$

where N represents the number of particles, l represents the index of each particle, and $\langle\cdot\rangle$ takes the average

over the corresponding ensemble. $\boldsymbol{r}$ is the coordinates of each particle which contain x and y components in 2-dimensional calculations and contain x, y, and z components in 3-dimensional calculations.

We first computed mean square displacement of zirconium and copper near the free surfaces, near the constrained surfaces, and in the bulk, and the results are shown in Figure 2.3. In the figure, the solid lines and the dotted lines show the 2-dimensional mean square displacement of atoms in the regions marked out by deep pink stripes in Figure 2.2. Notice that in these regions with a width of approximately 1 Å, the local atomic number density is larger than that in the bulk. The dash lines in the Figure 2.3 show the 3-dimensional mean square displacement in the bulk, which has been scaled by 2/3 in order to be compatible with the 2-dimensional results.

The involvement of mean square displacement can be divided into three regions governed by three different mechanisms including ballistic motion, cage effect, and diffusion, respectively. Firstly, within a short time period, particles move freely without interacting with each other due to the existence of the interval between them. This category of motion is referred to as ballistic motion [108]. That the mean square displacement is initially proportional to the time squared is a typical symbol of the ballistic motion. The cage effect originates from the interaction of particles with their neighbors. If the ballistic motion is impeded by the surrounding particles, the particle will be bounced back and rattle within the cage formed by its coordination particles. During the caging period, the growth of the mean square displacement slows down and exhibits a shoulder, and moreover, the width of the shoulder reflects the duration of the cage effect. Finally, once the structural relaxation breaks up the cage and induces the rearrangement of particles, the particle starts to diffuse within the system, and this procedure can be reflected from the characteristic that the mean square displacement becomes proportional to t again. In addition, the diffusion coefficient can be obtained from linear fitting to the mean square displacement in the diffusion domain by

$$D = \lim_{t\to\infty} \frac{|\boldsymbol{r}(t) - \boldsymbol{r}(0)|^2}{6t} \tag{2.5}$$

From Figure 2.3, we can clearly identify enhanced mobility near the free surfaces and a suppressed mobility near the constrained surfaces of $Zr_{50}Cu_{50}$ supercooled metallic liquid. $t < 0.1$ ps corresponds to the ballistic motion domain. During this period, the dash lines and the dotted lines overlap with each other, indicating $\langle \Delta^2 \boldsymbol{r} \rangle \propto t^2$ and dynamics of atoms have little difference in the bulk and near the constrained surface. However, the tail of ballistic motion is obviously longer near the free surfaces, indicating that the average cage size is larger. Notice that the local density near the free surfaces is even larger than that in the bulk, so here emerges a counter-intuitive phenomenon that the regions with higher density and less free

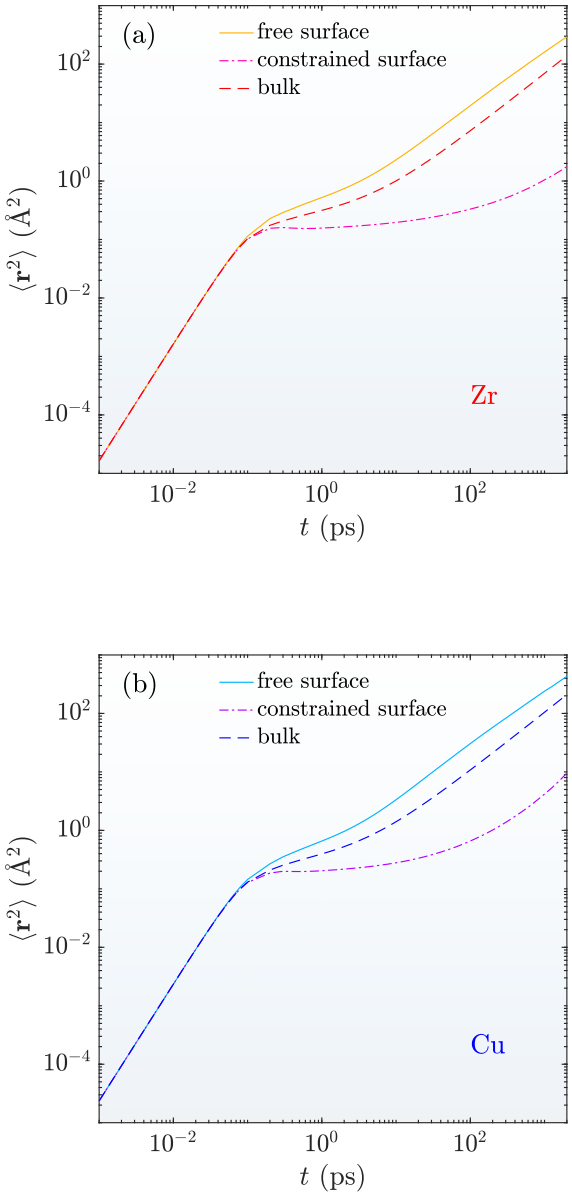

Figure 2.3: Mean square displacement near the free surfaces, near the constrained surfaces, and in the bulk of (a) zirconium and (b) copper atoms in $Zr_{50}Cu_{50}$ supercooled metallic liquid at 900K. The solid lines and the dotted lines represent the in-plane 2-dimensional mean square displacement of atoms near the free surface and near constrained surface respectively in the regions marked out by deep pink stripes in Figure 2.2. In these regions, the local atomic number density is larger than that in the bulk. The dash lines represent the 3-dimensional mean square displacement in the bulk scaled by 2/3.

volume have the larger cage size. From approximately $t = 0.1$ ps, all of the three lines bend downwards and exhibit shoulders with various widths, indicating the onset of the caging period. Near the constrained surfaces, the shoulder extends until about $t = 10^2$ ps, which is excessively wider than the shoulder either near the free surfaces or in the bulk. Thus, the cage effect near the constrained surfaces is the strongest and the relaxation of the system is the slowest. Near the free surfaces, the caging period ends slightly earlier than that in the bulk. Therefore, dynamics near the free surface is faster than dynamics in the bulk, either of which greatly exceeds dynamics near the constrained surfaces, despite the fact that the local structure near the free surfaces is more compact.

2.4 Velocity Autocorrelation Function

While mean square displacement reflects the dynamics in a long time scale, the velocity autocorrelation function is employed to describe the dynamics in a short time scale. The velocity autocorrelation function is a time-dependent correlation function computed by

$$C_{vv}(t) = \langle \boldsymbol{v}_i(0)\boldsymbol{v}_i(t)\rangle \tag{2.6}$$

where $\boldsymbol{v}_i$ is the velocity of each particle which contains x and y components in 2-dimensional calculations and contains x, y, and z components in 3-dimensional calculations, and $\langle\cdot\rangle$ takes the average over all atoms and over the corresponding ensemble. At $t = 0$, the absolute value of the velocity autocorrelation function provides information about the average kinetic energy of each particle. As time goes on, the velocity autocorrelation function decreases due to the loss of velocity autocorrelation of particles. It can become negative in a highly compact system since the cage effect bounces back particles from ballistic motion. Therefore, the depth of the negative part of the velocity autocorrelation function represents the intensity of the cage effect. As time goes to infinity, the velocity autocorrelation function is supposed to converge to 0 in liquids if the system is ergodic. The remaining oscillation around 0 at large t is induced by collective motions of the particles in the system referred to as "phonons" and damping fast in liquids [109].

We computed the velocity autocorrelation function of zirconium and copper near the free surfaces, near the constrained surfaces, and in the bulk of $Zr_{50}Cu_{50}$ supercooled liquid respectively. Figure 2.4 shows the results normalized by the corresponding values at $t = 0$. The solid lines and the dotted lines represent the in-plane 2-dimensional velocity autocorrelation function of atoms in the regions marked out by deep pink stripes in Figure 2.2. The dash lines represent the 3-dimensional velocity autocorrelation function in the bulk. As can be observed in the figure, the velocity autocorrelation function goes negative deeply near the

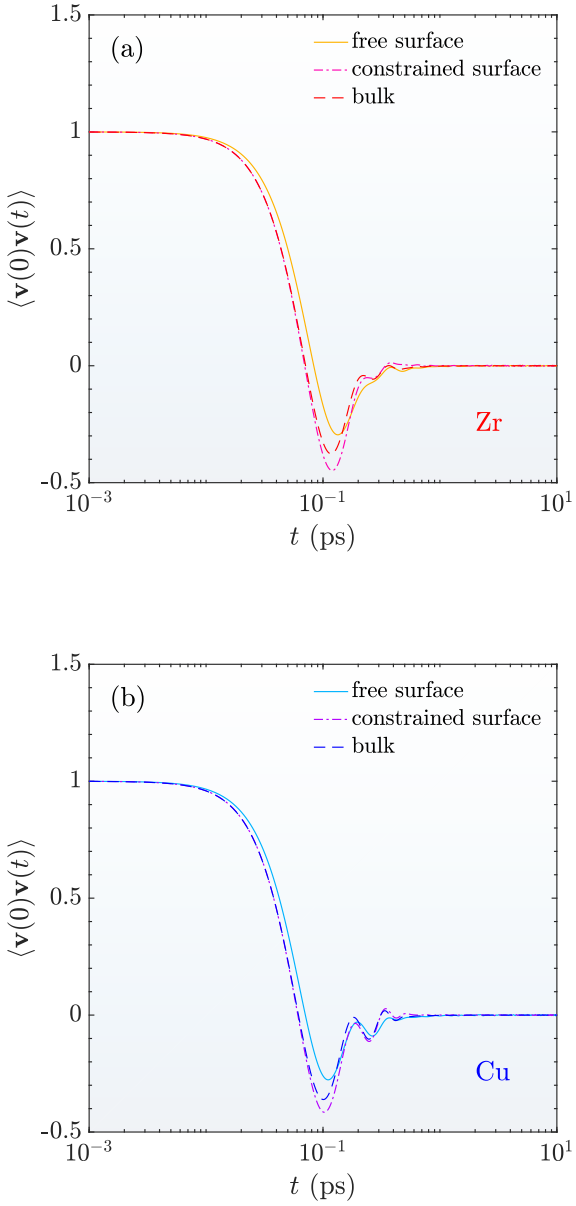

Figure 2.4: Velocity autocorrelation function normalized by $\langle \boldsymbol{v}_i(0)^2 \rangle$ near the free surfaces, near the constrained surfaces, and in the bulk of (a) zirconium and (b) copper in $Zr_{50}Cu_{50}$ supercooled metallic liquid at 900 K. The solid lines and the dotted lines represent the in-plane 2-dimensional velocity autocorrelation function of atoms in the regions marked out by deep pink stripes in Figure 2.2. In these regions, the local density is larger than that in the bulk. The dash lines represent the 3-dimensional velocity autocorrelation function in the bulks.

constrained surfaces but shallowly near the free surfaces. Therefore, the cage effect near the free surfaces is the weakest despite the highest local density and the most compact structure, which is consistent with our previous observation in mean square displacement. As time goes on, the velocity autocorrelation function near the free surfaces attenuates faster, indicating easier damping of phonons. On the other hand, the situation near the constrained surfaces is throughout the opposite to the situation near the free surfaces: the velocity autocorrelation function goes negative deeply and the oscillation at long time scale decays slowly. Therefore, the dynamics near the constrained surfaces are tightly restrained and more locally, while the dynamics near the free surfaces are largely enhanced and spreads widely.

2.5 Phonon Density of States

Since the oscillation of velocity autocorrelation function is induced by the phonons in the system, we can also examine the phonon behaviors through phonon (or vibrational) density of states via Fourier transforming velocity autocorrelation function into frequency domain as following [108]

$$\rho(\omega) = \frac{1}{2\pi} \int_{-\infty}^{\infty} \langle \boldsymbol{v}_i(t) \boldsymbol{v}_i(0) \rangle e^{-i\omega t} dt \tag{2.7}$$

In Equation 2.7, the phonon density of states is described as a function of frequency ω, nevertheless, it is usually expressed as a function of energy E in practice since it can be directly compared with experimental data obtained from inelastic neutron scattering.

Figure 2.5 shows the phonon density of states of zirconium and copper in $Zr_{50}Cu_{50}$ supercooled liquid near the free surfaces, near the constrained surfaces, and in the bulk. The results have been normalized by dividing the vibrational degree of freedom, that is, dN, where d is the dimension and N is the number of atoms. Firstly, the phonon density of states shifts towards domain with higher energy from in the bulk to near the constrained surfaces, which can be explained by that the dynamics near the constrained surfaces are more localized and therefore the phonon frequency is higher. However, the phonon density of states shifts towards domain with lower energy near the free surfaces although the local density is larger. Typically in a highly compact system, the phonon density of states tends to shift towards high-frequency domain because of the reduction of free volume. In this case, the enhanced dynamics near the free surfaces strengthens the relaxation processes which accelerates the structural rearrangement and the breaking of cages. Those effects surpass the effect of higher local density and speed up the damping of phonons with high frequencies, and therefore, the overall effect on phonon density of states near the free surfaces shifts it towards domain with lower energy.

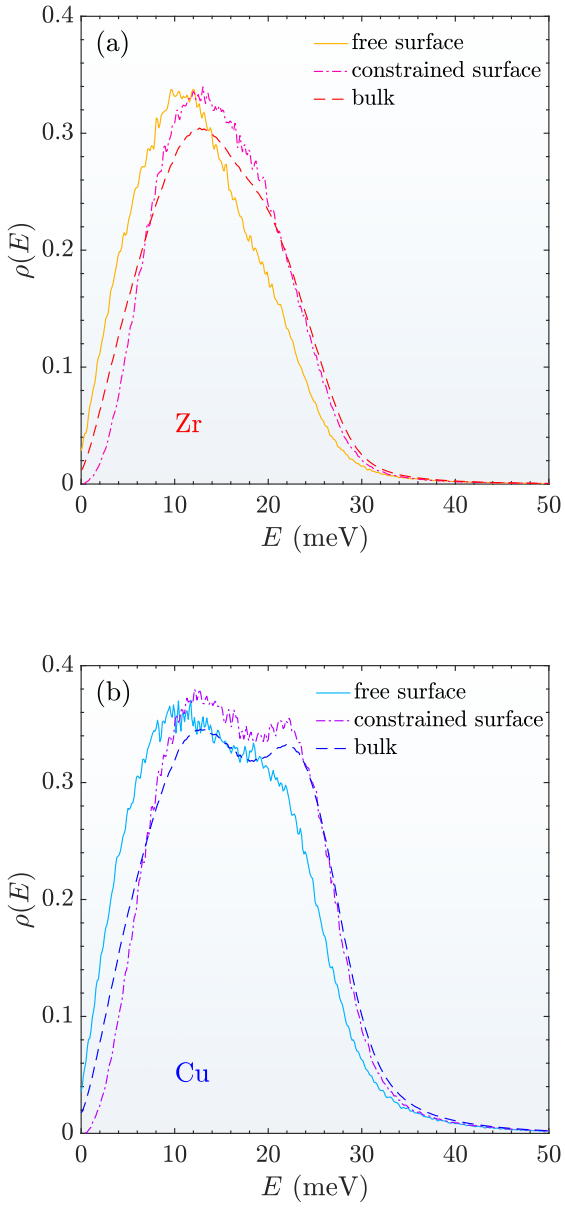

Figure 2.5: Normalized phonon density of states near the free surfaces, near the constrained surfaces, and in the bulk of (a) zirconium and (b) copper in $Zr_{50}Cu_{50}$ supercooled metallic liquid at 900K. The solid lines and the dotted lines represent the 2-dimensional in-plane phonon density of states in the regions marked out by deep pink stripes in Figure 2.2. In this region, the local density is larger than that in the bulk. The dash lines represent the 3-dimensional phonon density of states in the bulk.

2.6 Diffusion Coefficient and Mobility Gradient

Our previous discussion based on density profile, mean square displacement, velocity autocorrelation function and phonon density of states qualitatively identify enhanced mobility near the free surfaces which is independent with the fluctuation of local density. Therefore, the hypothesis that the enhanced dynamics near the free surfaces originates from larger local free volume may not tell the whole story. However, there is a lack of quantitative analysis of mobility gradient near the free surfaces, that is, how intensively the mobility increases near the free surfaces and how depth the enhanced mobility can penetrate into the bulk. In the following content, we demonstrate our calculation of diffusion coefficient at different depths from the surfaces which provides a quantitative profile of mobility gradient.

Diffusion coefficient D contains information about the mobility of particles in the system, which can be correlated with the relaxation process via fractional Stokes-Einstein relation [110]

$$D \propto (\tau/T)^{-\beta} \tag{2.8}$$

where τ represents the structural relaxation time and β is a species-dependent parameter typically ranging from 0.6 to 0.9 [111, 112, 113, 114, 115]. In our calculations, D was calculated by integrating velocity autocorrelation function according to Green-Kubo relation [116]

$$D = \frac{1}{d}\int_0^\infty \langle \boldsymbol{v}_i(t)\boldsymbol{v}_i(0)\rangle dt \tag{2.9}$$

where d is the dimension. Notice that D is equivalent to the value of $\rho(\omega)$ at $\omega = 0$ since diffusion can be regarded as the limit of vibration with infinitely low frequency.

In our work, we computed the 2-dimensional in-plane diffusion coefficient of zirconium and copper as a function of depth to the free surfaces and to the constrained surfaces in $Zr_{50}Cu_{50}$ supercooled liquid and the results are shown in Figure 2.6. The solid lines in the figure are the reference value of the 3-dimensional diffusion coefficient in the bulk system scaled by 2/3, and the dash lines are the fitting of D as a function of z near the free surface according to the RFOT theory [79]. From the figure, we observe that the surface effect can penetrate around 10 Å into the bulk, from where the diffusion starts to increase near the free surfaces and decrease near the constrained surfaces. Near the free surfaces, ROFT theory provides an analytical form of relaxation gradient as

$$\tau^{-1}(z) = (\tau_{\text{surf}}^{-1} - \tau_{\text{bulk}}^{-1})e^{z/\xi} + \tau_{\text{bulk}}^{-1} \tag{2.10}$$

where τ_{surf} and τ_{bulk} are the structural relaxation time on the surface and in the bulk respectively, and ξ is

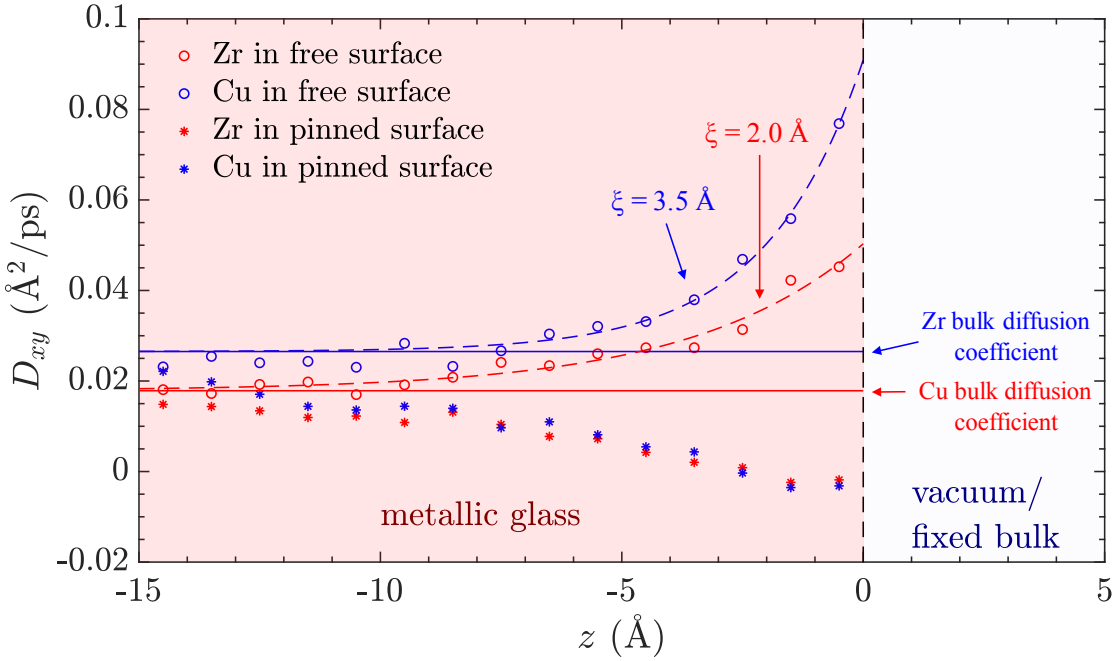

Figure 2.6: 2-dimensional diffusion coefficient along the x- and the y-directions of zirconium and copper as a function of depth to the free and the constrained surfaces in Zr_50Cu_{50} supercooled metallic liquid at 900 K. The solid lines represent the 3-dimensional diffusion coefficient in the bulk system and are scaled by 2/3. The dash lines represent the exponential fitting to the diffusion coefficients in the system with free surfaces according to the RFOT theory.

the dynamic correlation length [117]. Considering the inverse relation between D and τ, we can express the mobility gradient as

$$D(z) = (D_{\text{surf}} - D_{\text{bulk}})e^{z/\xi} + D_{\text{bulk}} \tag{2.11}$$

by taking $\xi = 1$ in Equation 2.8. The dash lines in Figure 2.6 show good fitting results according to Equation 2.11. The D of zirconium was fitted by

$$D_{\text{Zr}} = (0.050 - 0.018)e^{z/3.5} + 0.018 \tag{2.12}$$

and the D of copper was fitted by

$$D_{\text{Cu}} = (0.091 - 0.027)e^{z/2.0} + 0.027 \tag{2.13}$$

According to the fitting, the diffusion coefficient on the free surfaces is larger than that in the bulk approximately 2.8 times for zirconium and 3.4 times for copper. That the mobility of copper surpasses the mobility of zirconium can be explained by the radius difference between zirconium atoms and copper atoms. With a smaller radius, copper is more likely to flee from the cage effect and participates in long-range diffusion processes. In addition, the dynamic correlation lengths are approximately 3.5 Å for zirconium and 2.0 Å for copper, which are about 1.5 times of their Van der Waals radii respectively. Therefore, only the first layer of atoms near the free surfaces constitute a region with mobility enhanced collectively. This enhanced mobility can penetrate into the bulk due to the reduction of collective elasticity but decay exponentially, which is also accordance with the latest theoretical works [81]. On the other hand, the mobility decreases to zero when approaches the constrained surfaces. Obviously, the fixed boundaries restrain the motion of atoms adjacent to the constrained surfaces by friction and affect the inner atoms by enforced elasticity.

2.7 Out-of-Plane Motions

Our previous discussion only takes in-plane motions of atoms into consideration, nevertheless, out-of-plane motions in the z-direction may also contribute to the enhanced mobility near the free surfaces. In order to characterize out-of-plane motions, we introduced the exchange rate defined as the ratio of atoms in a certain layer transferring to an adjacent layer in a specific time interval. The exchange rate represents the frequency of atoms transferring between different layers. Therefore, it is proportional to the intensity of the motions in the z-direction.

Figure 2.7 shows the exchange rates of zirconium and copper respectively. The blue bars represent the

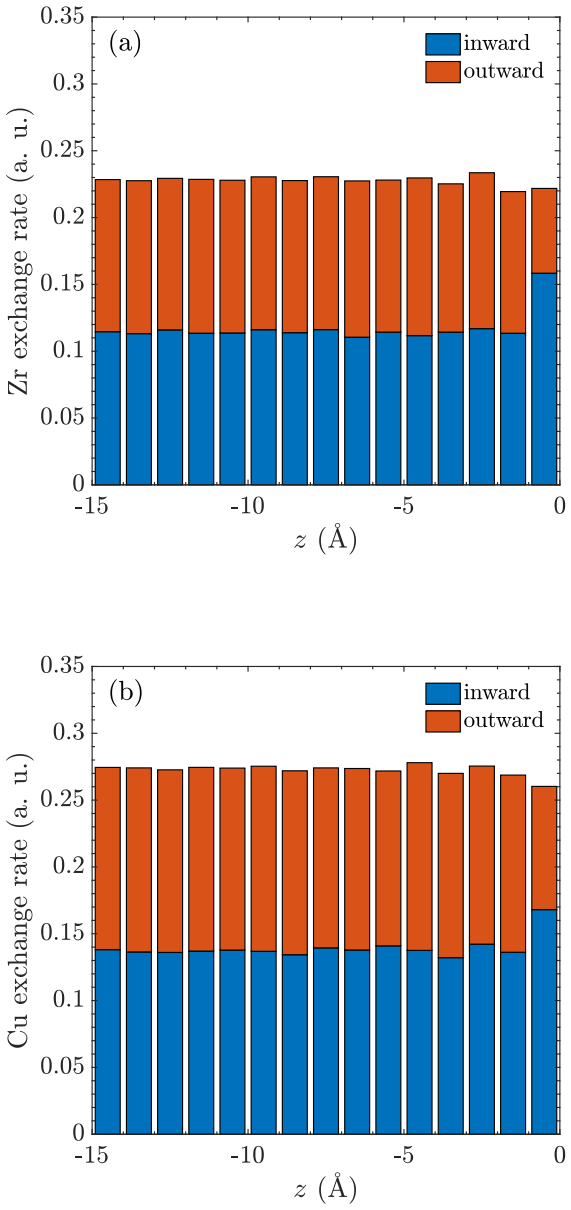

Figure 2.7: Inward and outward out-of-plane exchange rate of zirconium and copper atoms between layers as a function of depth to the free surfaces in $Zr_{50}Cu_{50}$ supercooled metallic liquid at 900 K.

inward exchange rate, that is, the rate of atoms in a certain layer transferring to its interior neighboring layer. In contrast, the outward exchange rate means the exchange of atoms to its exterior neighboring layer. For the outmost layer where the local density is smaller than the average bulk value, the inward exchange rate is larger than the outward exchange rate, indicating attractive interaction predominates in this region. As a consequence of the lower density and lack of coordinates, the mobility in this region is no wonder enhanced. However, the enhanced mobility still exists in the second layer close to the free surfaces even though the local density is larger and the atomic stacking is more compact. From the figure, it is hard to identify a distinction between the exchange rate in the second layer and in the bulk. The overall exchange rate in the second layer is approximately equal to that in the inner layers, and also the inward and outward exchange rates in the second layer are almost equivalent. Therefore, the atoms in the second layer do not have an obvious enhanced out-of-plane mobility propensity and do not have a preferred direction of out-of-plane motion. According to the discussion, we can eliminate a possible origin of the enhanced mobility near the free surfaces called the "skating" mechanism that particles can occasionally extract themselves from the bulk and move rapidly across the free surfaces until they get re-immersed into the dense phase. Comparing to adatom diffusion in the lattice which has fixed activation energy, the skating mechanism has a widely distributed activation energy due to the complexity of the energy landscape in amorphous materials. Therefore, the staking can persist in much lower temperatures if the surface maintains amorphous. This finding is consistent with the calculation that compares the diffusions including and excluding those skating particles near the free surface [43]. Therefore, we conclude that there is no evidence that the out-of-plane motion contributes to the enhanced mobility near the free surfaces and it can only originate from the collective in-plane motions even though the local structure could be more compact. This counter-intuitive phenomenon proves that, near the free surfaces, the dynamics of atoms are enhanced collectively rather than locally. Considering that if the surface is constrained, the mobility will become zero on the surface as a consequence of transverse friction and restriction enforced by those pinned atoms. Therefore, we can explain the enhanced mobility near the free surfaces by the vanished constraints and friction from the outside atoms. The out-of-plane constrain actually contributes little to the enhanced surface mobility. Instead, the vanishing of in-plane constraint can be the predominant reason, because attractive interaction near the free surface prevents the atoms from skating via vacuum and the in-plane mobility is predominantly enhanced.

2.8 Conclusions

In this work, we performed MD simulations on $Zr_{50}Cu_{50}$ supercooled metallic liquid in the bulk, near the constrained surfaces, and near the free surfaces at 900 K. Our calculations of mean square displacement and diffusion coefficient show that, near the constrained surfaces, the mobility of atoms decreases to zero, nevertheless, near the free surfaces, although the local density can be even higher, the in-plane mobility is approximately 3 times greater than that in the bulk. Further examination of velocity autocorrelation function identifies obstructed dynamics near the constrained surfaces with everlasting cage effect and a boosted dynamics near the free surfaces with early termination of the cage effect. The enhanced mobility near the free surfaces accelerates the damping of high-frequency phonons, and therefore, shifts the distribution of phonon density of states towards lower energy domain. In contrast, localized dynamics near the constrained surfaces alters the distribution of phonons to a higher energy domain. In addition, we computed the in-plane diffusion coefficient as a function of depth to the surfaces to characterize the mobility gradient. RFOT theory provides an exponential form of the mobility gradient near the free surfaces which fits well to out results. Finally, we calculated the atomic exchange rate between layers and found that the enhanced mobility near the free surfaces cannot be contributed by out-of-plane motions or "skating" atoms on the surfaces. Instead, in-plane motions should predominate the mobility near the free surfaces. Therefore, we conclude that the enhanced dynamics near the free surfaces should be collective and nearly independent with local density. Besides, the mechanism of enhanced dynamics near the free surfaces is the elimination of obstruction from those missing coordinations which enhances in-plane motions rather than out-of-plane motions of atoms on the surfaces. Our finding fills in the gap of understanding the mechanism of enhanced dynamics near the free surfaces of supercooled liquids or glasses. It directly testifies the prediction of existing theories such as RFOT theory on the dynamics gradient near the free surfaces. Finally, it gives insight to quantitatively adjust the dynamics near the free surfaces which is applicable in the real industry such as vapor deposition to produce ultrastable glasses.

Chapter 3

Temperature-Dependent Dynamics and Dynamic Heterogeneity in Supercooled Metallic Liquid

In this chapter, we study the temperature dependence of dynamics and dynamic heterogeneity of $Zr_{50}Cu_{50}$ supercooled liquid in the bulk and near the free surface using classical MD simulations. We calculated the dependence of diffusion coefficient on temperature and depth to the free surfaces. By fitting the mobility gradient to Equation 2.11, we extracted out-of-plane dynamic correlation length near the free surfaces as a function of temperature. Besides, we examined the dynamic heterogeneity as a function of temperature and depth by computing 2-dimensional non-Gaussian parameter [118]. Suprisingly, we observed a stronger dynamic heterogeneity of the outmost atomic layer on the free surface and a weaker dynamic heterogeneity in the bulk, which is contradictory with the prediction of existing theory. By correcting the assumption made by RFOT theory near the free surface, we explain this extra dynamic heterogeneity as the particularity of local environment of the outmost atomic layer. Due to the missing of unilateral neighboring atoms and the enhanced in-plane dynamics, the rearranging region on the free surface deforms from RFOT-predicted hemisphere to semi-ellipsoid, which extends the in-plane dynamic correlation length, and therefore, strengthens the dynamic heterogeneity on the free surface.

3.1 Method

In this study, we performed MD simulations on $Zr_{50}Cu_{50}$ supercooled liquid slabs with two free surfaces at different temperatures from 900 K to 1200 K with an interval of 20 K, that is, a total of 21 systems at different target temperatures were carried out. For each system, 20000 zirconium atoms and 20000 copper atoms were placed in cuboid boxes with periodic boundary conditions enforced in all three dimensions.

Before carrying out simulations, we determined the corrected density of each system at various temperatures by simulating the corresponding bulk system. The initial dimensions of the simulation boxes were set to $45.0 \times 45.0 \times 45.0$ Å^3. Enforced in the NPT ensemble, each system was equilibrated at 2000 K for 1 ns and quenched to the corresponding target temperature with a cooling rate of 10^{12} K/s. After equilibrated for 5 ns in the NPT ensemble, each system was then carried out for another 5 ns, during which the density

was collected and averaged to obtain the corrected density.

Figure 3.1 shows the corrected density of $Zr_{50}Cu_{50}$ supercooled liquid between 900 K to 1200 K. The density as a function of temperature was fitted well by a quadratic form

$$\rho(T) = 6.543955^{-10}T^2 - 4.729302 \times 10^{-6}T + 5.913360 \times 10^{-2} \tag{3.1}$$

In our simulations, the setup of each system was almost the same as shown in Figure 2.2(b), except the dimensions. For each system, the side length of the simulation boxes in the z-direction was set to 40.0 Å, and the side lengths in the x- and the y-directions were set to be equivalent and determined from the corrected density calculated from Equation 3.1 according to the target temperature. All of the following simulations were performed in the NVT ensemble. Each system was first equilibrated at 2000 K for 1 ns, then, quenched to the target temperature with a cooling rate of 10^{12} K/s. After the system had been well equilibrated for 5 ns, the simulation box was doubly enlarged in the z-direction and two free surfaces perpendicular to the z-axis were created. Two vacuum volumes were reserved to eliminate the interaction from periodic images. Finally, the system was equilibrated for another 5 ns before ready to generate simulation trajectories.

Simulation parameters including integration time step and algorithm, trajectory dumping strategy, force field, and temperature and pressure control algorithms were the same as described in Chapter 2. All of the simulations were also carried out using LAMMPS [99] and part of the trajectory analysis was performed using LiquidLib [104].

The target temperatures of our simulations range from 900 K to 1200 K which largely exceed the glass transition temperature of the system (677 K). Besides, we well equilibrated the systems for at least 5 ns before collecting trajectories. Therefore, the ergodicity of our simulation can be guaranteed. In the calculation of each quantity, we took an ensemble average of at least 50000 frames, which was supposed to well represent the real ensemble. Therefore, the uncertainty, which only originates from the round-off error of the computation device and the error that we assume our trajectory can well represent the real ensemble, is supposed to be negligible in our calculations.

3.2 Temperature and Depth Dependent Dynamics

We first calculated the diffusion coefficient of zirconium and copper individually as a function of temperature and depth to the free surfaces by integrating velocity autocorrelation function (Equation 2.5). The results are plotted as heat maps and shown in Figure 3.2. From the figure, we clearly identify enhancement of diffusion near the free surfaces and at higher temperatures. The copper atoms are universally more diffusive

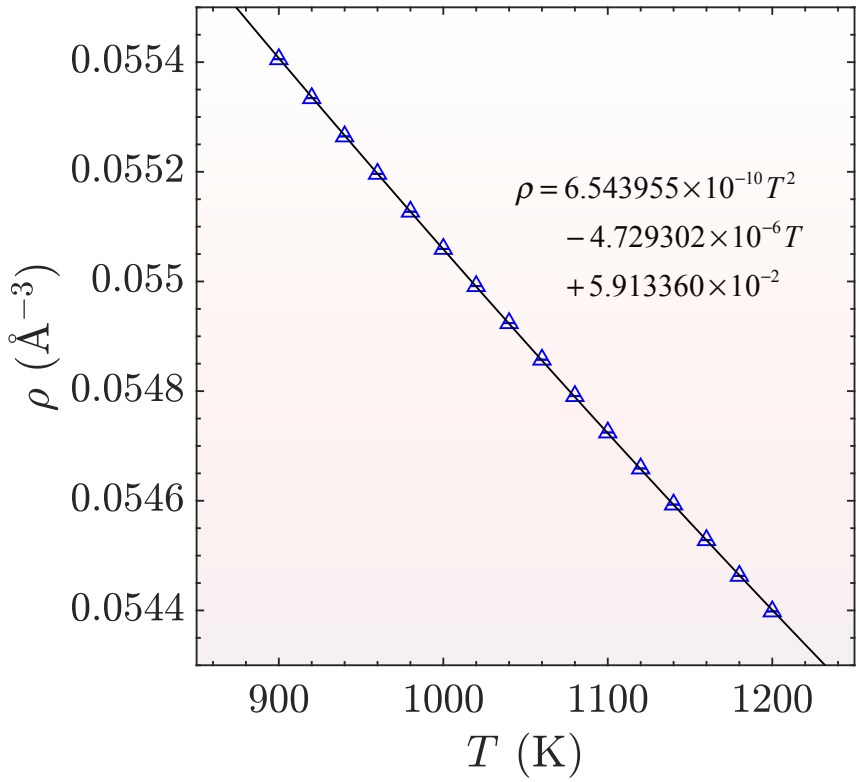

Figure 3.1: The density of $Zr_{50}Cu_{50}$ supercooled metallic liquid obtained at various temperature by MD simulations in the NPT ensemble. The black line shows a quadratic fitting of the density to temperature.

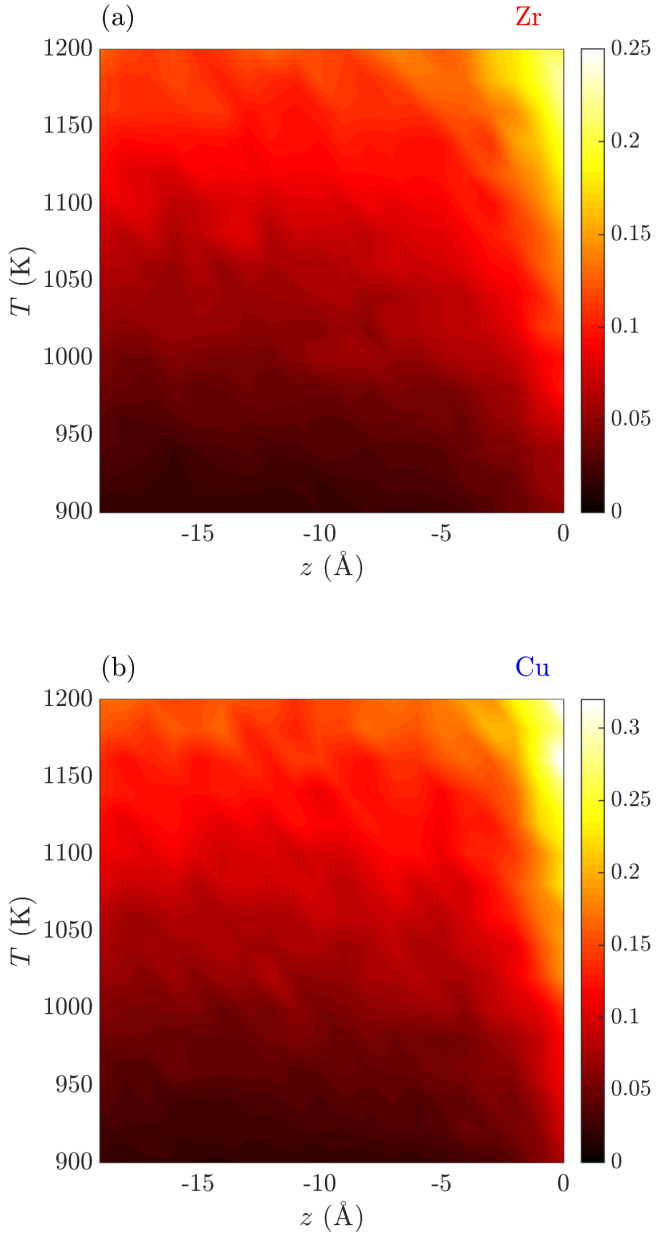

Figure 3.2: Diffusion coefficient of (a) zirconium and (b) copper in $Zr_{50}Cu_{50}$ supercooled metallic liquid as a function of temperature and depth to the free surfaces plotted as heat maps. The unit of color bars is $Å^2/ps$.

than the zirconium atoms, which can be explained by the larger size of the zirconium atom. As temperature increases, the contrast of diffusion near the free surfaces and in the bulk decreases, indicating the effect of enhanced dynamics is more drastic at lower temperatures. This observation is consistent with the reports that the mobility near the free surfaces can be several orders of magnitude larger than the mobility in the bulk when it approaches T_g [38, 39, 40, 41, 42, 43, 44]. However, the temperature near T_g is inaccessible by classical MD simulation as a consequence of the exponentially increasing structural relaxation time with temperature decreasing. Therefore, enhanced sampling techniques must be employed in the future study if we want to reach the temperature domain near or even below T_g.

By fitting the diffusion coefficient as a function of depth to the free surfaces according to Equation 2.11 at each temperature, we extracted out-of-plane dynamic correlation length ξ as a function of temperature and plotted in Figure 3.3. Out-of-plane dynamic correlation length, in this case, represents how deep the enhanced dynamics near the free surfaces can penetrate into the bulk. Taking errors into consideration, the out-of-plane dynamic correlation length does not possess a temperature-dependent obviously. For either zirconium or copper, the out-of-plane dynamic correlation length is approximately 1.3 times greater than its radius, which means, the enhanced dynamics can only effectively affect the first atomic layer on the free surfaces. Since the atomic radii of zirconium and copper will not change significantly with temperature increasing, the out-of-plane dynamic correlation length, therefore, shows little temperature dependence in the temperature range we studied. At low temperatures, the characteristic relaxation time scale exceeds the capability of classical MD simulations. Therefore, more advanced sampling method should be utilized to probe the structural and dynamic properties under low-temperature condition. This finding is consistent with our previous conclusion in Chapter 2.

3.3 Temperature and Depth Dependent Dynamic Heterogeneity

Besides the dynamic properties, we further examined the dynamic heterogeneity in the system as a function of temperature and depth to the free surfaces. In a homogeneous system, the diffusion or the stochastic displacements of the particles should follow a Gaussian distribution [119]. However, when the dynamics in a system are heterogeneous, the Gaussian distribution no longer works for diffusion. In this case, the non-Gaussian parameter and its maximum value are usually adopted to quantify the dynamic heterogeneity of a supercooled liquid or glass [118, 120]. The non-Gaussian parameter is defined by the following equation [121]

$$\alpha_{2,d}(t) = \frac{d\langle \boldsymbol{r}^4(t)\rangle}{(d+2)\langle \boldsymbol{r}^2(t)\rangle^2} - 1 \tag{3.2}$$

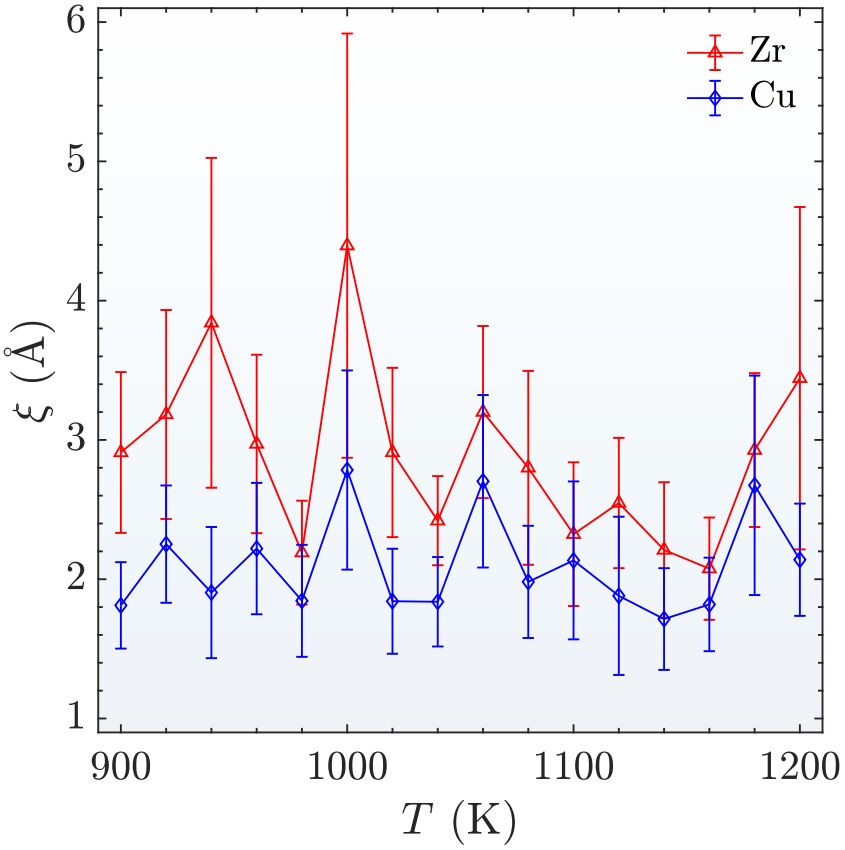

Figure 3.3: Dynamic correlation length near the free surfaces of $Zr_{50}Cu_{50}$ supercooled metallic liquid as a function to temperature obtained from fitting diffusion coefficient according to Equation 2.11.

where d is the calculation dimension, $\boldsymbol{r}(t)$ represents the displacement of particles at time t, and $\langle\cdot\rangle$ is the ensemble average. Since our computation only took in-plane motion into consideration, $d = 2$ was adopted over the computation. $\alpha_2(t)$ reflects the deviation of the statistics of diffusion from a Gaussian distribution. $\alpha_2(t) = 0$ means the diffusion follows Gaussian distribution and the dynamics of the system is homogeneous. In contrast, $\alpha_2(t) \neq 0$ indicates a heterogeneous dynamics in the system and the maximum value of $\alpha_2(t)$, $\alpha_{2,\max}$ describes the degree of this deviation.

Figure 3.4 shows the 2-dimensional $\alpha_2(t)$ of zirconium and copper at 1100 K. Each line represents the $\alpha_2(t)$ within a certain layer with a width of 1 Å in the z-dircetion. The depths to the free surfaces range from 19.5 to 0.5 Å, and the lighter the color of a line, the closer the corresponding layer is to the free surfaces. From the figure, we can observe an unexpected non-monotonic trend of $\alpha_{2,\max}$ with z increasing. To be specific, from the bulk to the surfaces, $\alpha_{2,\max}$ first gradually decreases, indicating a more homogeneous dynamics approaching to the free surfaces. However, $\alpha_{2,\max}$ suddenly increases at the outmost three layers showed by the three lines with the lightest color, which means, dynamic heterogeneity has an abrupt increment near the free surfaces. RFOT theory regards the mechanism of the enhanced surface mobility as the shortening of dynamic correlation length, thus, it predicts that the dynamics near the free surface should be less heterogeneous [1, 79]. Nevertheless, our observation shows that, rather than weakened, the dynamic heterogeneity near the free surfaces is even enhanced. Therefore, there must be additional mechanisms accounting for the simultaneous enhancement of both dynamics and dynamic heterogeneity near the free surface.

To identify the dependence of dynamic heterogeneity on the depth to the free surfaces, we plotted $\alpha_{2,\max}$ of zirconium and copper as a function of temperature T and depth z as heat maps in Figure 3.5. The figure transparently indicates a region near the free surfaces with more heterogeneous dynamics than in the bulk. The width of the region changes from approximately 3 Å to 1.5 Å when temperature increases from 900 K to 1200 K. The degree of dynamic heterogeneity suddenly drops off below this region, and gradually rises back with z increasing. This counter-intuitive phenomenon unveils the particularity of the outmost atomic layer. For except the outmost atomic layer, dynamics strengthens and dynamic heterogeneity weakens with the depth decreasing, which is consistent with the predictions of the RFOT theory. However, the behaviors of the outmost atomic layer break this law. This violation between the theory and the observation does not indicate the invalidity of the RFOT theory. Instead, it illustrates that the assumption made by the RFOT theory near the free surface is oversimplified. Namely, the dynamic rearranging regions are spherical in the bulk and hemispherical near the free surface as assumed by the RFOT theory[79], nevertheless, our results and discussion in Chapter 2 have shown that the dynamics near the free surface is predominantly contributed

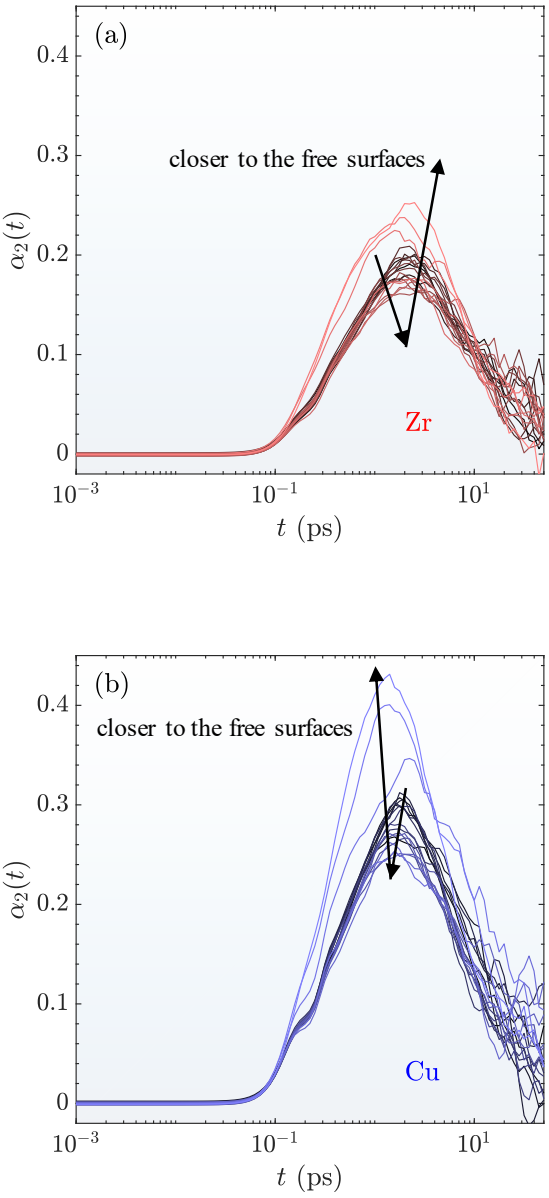

Figure 3.4: The non-Gaussian parameter $\alpha_2(t)$ of (a) zirconium and (b) copper at various depth to the free surfaces in $Zr_{50}Cu_{50}$ supercooled metallic liquid at 1100 K. Each line represents the 2-dimensional $\alpha_2(t)$ within a certain layer with a width of 1 Å. The lighter the color of a line, the closer the corresponding layer is to the free surfaces. The depths of the layers to the free surfaces range from 19.5 to 0.5 Å.

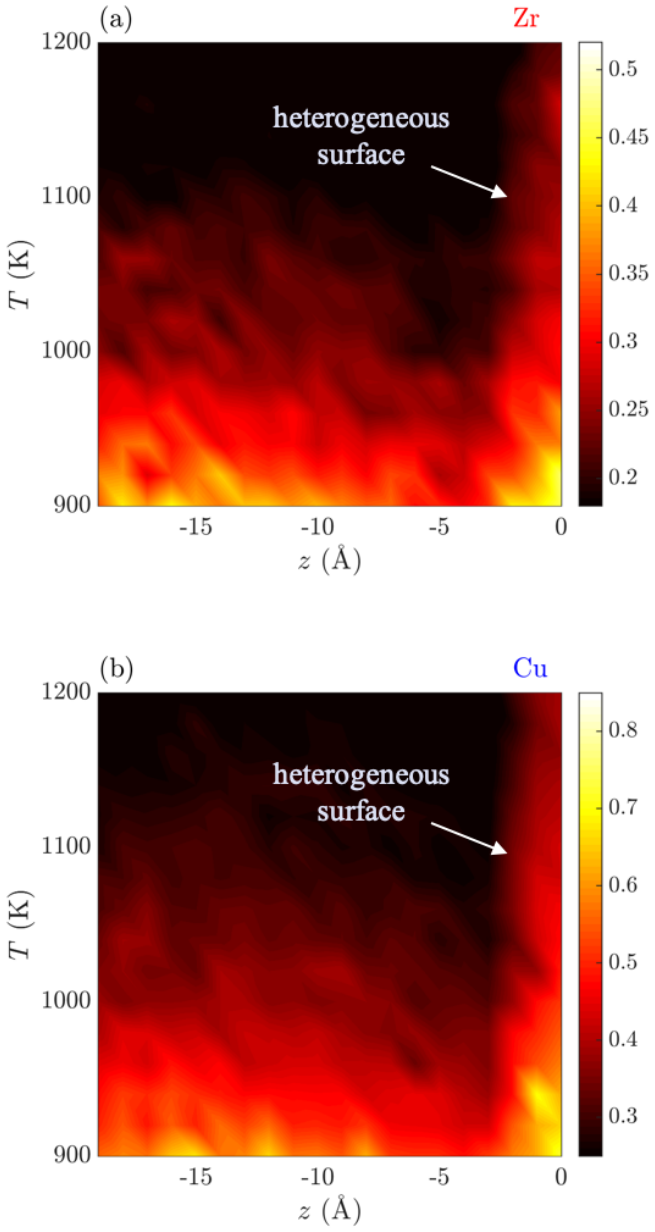

Figure 3.5: $\alpha_{2,\max}$ of (a) zirconium and (b) copper in $Zr_{50}Cu_{50}$ supercooled metallic liquid as a function of temperature and depth to the free surfaces plotted as heat maps.

by in-plane motions. Therefore, the rearranging region near the free surface should be a semi-ellipsoid with the long axis parallel to the free surface, which extends the dynamic correlation length and introduces extra dynamic heterogeneity on the free surface.

The particularity of the outmost atomic layer is also supported by the recent ECNLE theory [81]. Due to the missing neighboring atoms, the local environment of the first atomic layer is different from the environment in the bulk. The unilateral roughness brought by inner atoms creates tiny local structures that accelerate or hinder the in-plane motions of the surface atoms, thus, it introduces extra dynamic heterogeneity on the free surface. For other atoms, as a consequence of approximately isotropic local environment, the shape of the dynamic rearranging region is close to spherical. In this case, the RFOT theory can be applied suitably.

3.4 Conclusions

In this chapter, we study the temperature dependence of dynamics and dynamic heterogeneity of $Zr_{50}Cu_{50}$ supercooled liquid using classical MD simulations. The calculation of diffusion coefficient as a function of temperature and depth to the free surfaces identifies a temperature-independent out-of-plane dynamic correlation length near the free surfaces, the width of which can only cover the outmost atomic layer. The investigation of in-plane dynamic heterogeneity characterized by 2-dimensional $\alpha_{2,\max}$ reveals that the dynamics within the outmost atomic layer are more heterogeneous than that in the bulk, which is contradictory with the prediction made by the RFOT theory. Considering the finding that the dynamics near the free surface is only enhanced in the transverse direction in Chapter 2, we realize that the assumption made by the RFOT theory that the dynamic rearranging region near the free surface is hemispherical cannot describe the real physics appropriately. Instead, we argue that the dynamic rearranging region near the free surface is distorted from 3-dimension to 2-dimension as a consequence that the dynamics near the free surface is predominately contributed by in-plane motions. Therefore, the in-plane dynamic correlation length is extended and the dynamic heterogeneity is enhanced in the outmost atomic layer on the free surface.

Chapter 4

Summary and Future Work

In this work, we first performed MD simulations on $Zr_{50}Cu_{50}$ supercooled metallic liquid in the bulk, near the free surfaces, and near the constrained surfaces at a target temperature 900 K to figure out the mechanism of enhanced mobility near the free surface. The atomic motions in the system were examined separately as in-plane motions parallel to the interface and out-of-plane motions perpendicular to the interface. The in-plane dynamics near the free surface is shown to be faster than the dynamics in the bulk, although the local structure near the free surface can be even more compact. However, the investigation on the jumping rate of atoms shows that the out-of-plane dynamics on the free surface was almost the same or even weaker than that in the bulk. Mean square displacement and velocity autocorrelation function indicate that the cage effect terminates earlier and atomic rearrangement is more drastic near the free surface, which attenuates phonons with higher energy and shifts phonon density of states towards lower energy domain. In contrast, when the vacuum space is filled with pinned atoms, the mobility near the interface decreases to zero rapidly. These facts and phenomena conclude that the enhanced dynamics near the free surface does not originate from larger free volumes or skating atoms on the free surface. Instead, with missing coordination atoms in the vacuum space, the in-plane friction induced on those atoms on the free surface is halved, which finally strengthens the in-plane collective motions on the free surface.

Further on, we examined the temperature-dependence of dynamics and dynamic heterogeneity of $Zr_{50}Cu_{50}$ supercooled metallic liquid near the free surface. Dynamic heterogeneity can be reflected by the dynamic correlation length directly. The RFOT theory proposed that the enhanced dynamics near the free surface is induced by the shortening of the dynamic correlation length. Here, the out-of-plane dynamic correlation length extracted from fitting the relation between the diffusion coefficient and the temperature to Equation 2.11 shows little temperature dependence, which demonstrates the particularity of the outmost atomic layer on the free surface. However, the in-plane dynamic correlation length characterized by 2-dimensional $\alpha_{2,\max}$ was found to increase on the free surface. Considering the enhanced in-plane dynamics, we realize that the assumption made by RFOT theory that the dynamic rearranging region near the free surface is hemispherical is oversimplified. Instead, the dynamic rearranging region is distorted to semi-ellipsoid with

the long axis parallel to the free surface, which results in the counter-intuitive simultaneous enhancement of both dynamics and dynamic heterogeneity on the free surface.

This study unveils the mechanism of enhanced dynamics near the free surface of supercooled metallic liquid. It also reveals the defects of the existing theory describing the behaviors of dynamics and dynamic heterogeneity near the free surface. Therefore, this study offers insight into solving the mystery of the glass transition and even sheds light on the investigation of complicated relaxation processes in the glassy systems. On the other hand, it also provides simulational guidance for application relying on enhanced surface mobility, for example, the manufacture of ultrastable glasses by vapor deposition.

In future work, we will focus on the extension of this research and attempt to solve the problem remaining in this study. First, the energy landscape near the free surface is too complex to sample using classical MD simulations, and thus, it is hard to quantify the distribution of the activation energy of structure rearrangement. To solve this issue, we will utilize more advanced sampling methods, for instance, the Ascent Dynamics method developed by our group, to sample the energy landscape of the supercooled liquids at the free surface or in the bulk. Second, experimental evidence is still lacking to support simulation results and theoretical viewpoints. For example, our hypothesis that the rearranging region at the free surface is distorted to semi-ellipsoid is hard to be validated with existing experimental results. Neutron scattering experiment, whose measurement time scale covers the typical characteristic relaxation time scale of glasses and supercooled liquids, is a suitable technique to explore the dynamics in glasses or supercooled liquids. We may take advantage of this technique and design experiments to directly measure the surface dynamics and dynamic heterogeneity. Finally, the current force field describing the metallic glasses is not universal, especially for those elements with angular dependent interactions. Neural network potential [122], which reaches the first-principle accuracy at force field computational cost, can be a perfect extension of currently used classical force field. We hope to develop accurate neural network potentials for the systems we are interested in, to assist study the physical questions with the first-principle accuracy at classical MD cost.

References

[1] Vassiliy Lubchenko and Peter G. Wolynes. Theory of structural glasses and supercooled liquids. *Annual Review of Physical Chemistry*, 58:235–266, 2007.

[2] J. Frenkel. *Kinetic theory of liquids*. Oxford University Press, 1946.

[3] Johannes Diderik Van der Waals. *Over de continuiteit van den gas: en vloeistoftoestand*. Leiden University, 1873.

[4] David Turnbull. Under what conditions can a glass be formed? *Contemporary Physics*, 10(5):473–488, 1969.

[5] Ken Dill and Sarina Bromberg. *Molecular driving forces: Statistical thermodynamics in biology, chemistry, physics, and nanoscience*. Garland Science, 2012.

[6] Pablo G. Debenedetti and Frank H. Stillinger. Supercooled liquids and the glass transition. *Nature*, 410:259–267, 2001.

[7] Peter G. Wolynes. Entropy crises in glasses and random heteropolymers. *Journal of Research of the National Institute of Standards and Technology*, 102(2):187–194, 1997.

[8] M. D. Ediger and Peter Harrowell. Perspective: Supercooled liquids and glasses. *The Journal of Chemical Physics*, 137(8):080901, 2012.

[9] Walter Kauzmann. The nature of the glassy state and the behavior of liquids at low temperatures. *Chemical reviews*, 43(2):219–256, 1948.

[10] Pablo G. Debenedetti. *Metastable liquids: Concepts and principles*. Princeton University Press, 1996.

[11] C. A. Angell. Formation of glasses from liquids and biopolymers. *Science*, 267:1924–1935, 1995.

[12] C. A. Angell. Entropy and fragility in supercooling liquids. *Journal of Research of the National Institute of Standards and Technology*, 102(2):171–185, 1997.

[13] Andrew I. Mel'cuk, Raphael A. Ramos, Harvey Gould, W. Klein, and Raymond D. Mountain. Long-lived structures in fragile glass-forming liquids. *Physical Review Letters*, 75(13):2522–2525, 1995.

[14] Jacob D. Stevenson and Peter G. Wolynes. The ultimate fate of supercooled liquids. *The Journal of Physical Chemistry A*, 115(16):3713–3719, 2010.

[15] Theodore R. Kirkpatrick, Devarajan Thirumalai, and Peter G. Wolynes. Scaling concepts for the dynamics of viscous liquids near an ideal glassy state. *Physical Review A*, 40(2):1045–1054, 1989.

[16] M. Wolfgardt, J. Baschnagel, W. Paul, and K. Binder. Entropy of glassy polymer melts: Comparison between Gibbs-DiMarzio theory and simulation. *Physical Review E*, 54(2):1535–1543, 1996.

[17] Giulio Biroli and Juan P. Garrahan. Perspective: The glass transition. *The Journal of Chemical Physics*, 138(12):12A301, 2013.

[18] Jerzy Zarzycki. *Glasses and the vitreous state*. Number 9. Cambridge university press, 1991.

[19] L.-M. Martinez and C. A. Angell. A thermodynamic connection to the fragility of glass-forming liquids. *Nature*, 410(6829):663–667, 2001.

[20] Hans Vogel. Das temperatur-abhängigkeitsgesetz der viskosität von flüssigkeiten. *Physikalische Zeitschrift*, 22:645–646, 1921.

[21] Von G. Tammann and W. Hesse. Die Abhängigkeit der viscosität von der temperatur bie unterkühlten flüssigkeiten. *Zeitschrift für anorganische und allgemeine Chemie*, 156(1):245–257, 1926.

[22] Gordon S. Fulcher. Analysis of recent measurements of the viscosity of glasses. *Journal of the American Ceramic Society*, 8(6):339–355, 1925.

[23] C. Austin Angell, Kia L. Ngai, Greg B. McKenna, Paul F. McMillan, and Steve W. Martin. Relaxation in glassforming liquids and amorphous solids. *Journal of Applied Physics*, 88(6):3113–3157, 2000.

[24] T. Iwashita, Donald M. Nicholson, and Takeshi Egami. Elementary excitations and crossover phenomenon in liquids. *Physical Review Letters*, 110(20):205504, 2013.

[25] Mark D. Ediger. Spatially heterogeneous dynamics in supercooled liquids. *Annual Review of Physical Chemistry*, 51(1):99–128, 2000.

[26] Ranko Richert. Heterogeneous dynamics in liquids: Fluctuations in space and time. *Journal of Physics: Condensed Matter*, 14(23):R703–R738, 2002.

[27] J. R. Dutcher and M. D. Ediger. Glass surfaces not so glassy. *Science*, 319(5863):577–578, 2008.

[28] J. A. Forrest. What can we learn about a dynamical length scale in glasses from measurements of surface mobility? *The Journal of Chemical Physics*, 139(8):084702, 2013.

[29] Fei Chen, Chi-Hang Lam, and Ophelia K. C. Tsui. The surface mobility of glasses. *Science*, 343(6174):975–976, 2014.

[30] Kevin F. Mansfield and Doros N. Theodorou. Molecular dynamics simulation of a glassy polymer surface. *Macromolecules*, 24(23):6283–6294, 1991.

[31] Daisuke Kawaguchi, Keiji Tanaka, Tisato Kajiyama, Atsushi Takahara, and Seiji Tasaki. Mobility gradient in surface region of monodisperse polystyrene films. *Macromolecules*, 36(4):1235–1240, 2003.

[32] Z. Fakhraai and J. A. Forrest. Measuring the surface dynamics of glassy polymers. *Science*, 319(5863):600–604, 2008.

[33] Zhaohui Yang, Yoshihisa Fujii, Fuk Kay Lee, Chi-Hang Lam, and Ophelia K. C. Tsui. Glass transition dynamics and surface layer mobility in unentangled polystyrene films. *Science*, 328(5986):1676–1679, 2010.

[34] Keewook Paeng, Stephen F. Swallen, and M. D. Ediger. Direct measurement of molecular motion in freestanding polystyrene thin films. *Journal of the American Chemical Society*, 133(22):8444–8447, 2011.

[35] L. Zhu, C. W. Brian, S. F. Swallen, P. T. Straus, M. D. Ediger, and L. Yu. Surface self-diffusion of an organic glass. *Physical Review Letters*, 106(25):256103, 2011.

[36] Lian Yu. Surface mobility of molecular glasses and its importance in physical stability. *Advanced Drug Delivery Reviews*, 100:3–9, 2016.

[37] M. Tylinski, M. S. Beasley, Y. Z. Chua, C. Schick, and M. D. Ediger. Limited surface mobility inhibits stable glass formation for 2-ethyl-1-hexanol. *The Journal of Chemical Physics*, 146(20):203317, 2017.

[38] Zane Shi, Pablo G. Debenedetti, and Frank H. Stillinger. Properties of model atomic free-standing thin films. *The Journal of Chemical Physics*, 134(11):114524, 2011.

[39] Rohit Malshe, M. D. Ediger, Lian Yu, and J. J. De Pablo. Evolution of glassy gratings with variable aspect ratios under surface diffusion. *The Journal of Chemical Physics*, 134(19):194704, 2011.

[40] T. Q. Dong, V. V. Hoang, and Guy Lauriat. Molecular simulation of freestanding amorphous nickel thin films. *Thin Solid Films*, 545:584–591, 2013.

[41] Yu Chai, Thomas Salez, Joshua D. McGraw, Michael Benzaquen, Kari Dalnoki-Veress, Elie Raphaël, and James A. Forrest. A direct quantitative measure of surface mobility in a glassy polymer. *Science*, 343(6174):994–999, 2014.

[42] C. R. Cao, Y. M. Lu, H. Y. Bai, and W. H. Wang. High surface mobility and fast surface enhanced crystallization of metallic glass. *Applied Physics Letters*, 107(14):141606, 2015.

[43] Gang Sun, Shibu Saw, Ian Douglass, and Peter Harrowell. Structural origin of enhanced dynamics at the surface of a glassy alloy. *Physical Review Letters*, 119(24):245501, 2017.

[44] L. Chen, C. R. Cao, J. A. Shi, Z. Lu, Y. T. Sun, P. Luo, L. Gu, H. Y. Bai, M. X. Pan, and W. H. Wang. Fast surface dynamics of metallic glass enable superlatticelike nanostructure growth. *Physical Review Letters*, 118(1):016101, 2017.

[45] Shankar P. Das. Mode-coupling theory and the glass transition in supercooled liquids. *Reviews of Modern Physics*, 76(3):785–851, 2004.

[46] Kenneth L. Kearns, Stephen F. Swallen, Mark D. Ediger, Tian Wu, Ye Sun, and Lian Yu. Hiking down the energy landscape: Progress toward the Kauzmann temperature via vapor deposition. *The Journal of Physical Chemistry B*, 112(16):4934–4942, 2008.

[47] Sébastien Léonard and Peter Harrowell. Macroscopic facilitation of glassy relaxation kinetics: Ultrastable glass films with frontlike thermal response. *The Journal of Chemical Physics*, 133(24):244502, 2010.

[48] Ivan Lyubimov, Mark D. Ediger, and Juan J. de Pablo. Model vapor-deposited glasses: Growth front and composition effects. *The Journal of Chemical Physics*, 139(14):144505, 2013.

[49] Hai-Bin Yu, Yuansu Luo, and Konrad Samwer. Ultrastable metallic glass. *Advanced Materials*, 25(41):5904–5908, 2013.

[50] Mark D. Ediger. Perspective: Highly stable vapor-deposited glasses. *The Journal of Chemical Physics*, 147(21):210901, 2017.

[51] Yue Qiu, Shakeel S Dalal, and M. D. Ediger. Vapor-deposited organic glasses exhibit enhanced stability against photodegradation. *Soft Matter*, 14(15):2827–2834, 2018.

[52] M. D. Ediger and J. A. Forrest. Dynamics near free surfaces and the glass transition in thin polymer films: A view to the future. *Macromolecules*, 47(2):471–478, 2013.

[53] Yue Zhang and Zahra Fakhraai. Decoupling of surface diffusion and relaxation dynamics of molecular glasses. *Proceedings of the National Academy of Sciences*, 114(19):4915–4919, 2017.

[54] Asaph Widmer-Cooper and Peter Harrowell. Free volume cannot explain the spatial heterogeneity of Debye-Waller factors in a glass-forming binary alloy. *Journal of Non-Crystalline Solids*, 352(42-49):5098–5102, 2006.

[55] Asaph Widmer-Cooper and Peter Harrowell. Predicting the long-time dynamic heterogeneity in a supercooled liquid on the basis of short-time heterogeneities. *Physical Review Letters*, 96(18):185701, 2006.

[56] Martin Goldstein. Viscous liquids and the glass transition: A potential energy barrier picture. *The Journal of Chemical Physics*, 51(9):3728–3739, 1969.

[57] Hans Frauenfelder, Stephen G. Sligar, and Peter G. Wolynes. The energy landscapes and motions of proteins. *Science*, 254(5038):1598–1603, 1991.

[58] J. G. Saven, J. Wang, and P. G. Wolynes. Kinetics of protein folding: the dynamics of globally connected rough energy landscapes with biases. *The Journal of Chemical Physics*, 101(12):11037–11043, 1994.

[59] V. I. Abkevich, A. M. Gutin, and E. I. Shakhnovich. Free energy landscape for protein folding kinetics: Intermediates, traps, and multiple pathways in theory and lattice model simulations. *The Journal of Chemical Physics*, 101(7):6052–6062, 1994.

[60] Jin Wang, Jose Onuchic, and Peter Wolynes. Statistics of kinetic pathways on biased rough energy landscapes with applications to protein folding. *Physical Review Letters*, 76(25):4861–4864, 1996.

[61] Jianhui Tian and Angel E. Garcia. Simulation studies of protein folding/unfolding equilibrium under polar and nonpolar confinement. *Journal of the American Chemical Society*, 133(38):15157–15164, 2011.

[62] Kristen A. Marino and Peter G. Bolhuis. Confinement-induced states in the folding landscape of the Trp-cage miniprotein. *The Journal of Physical Chemistry B*, 116(39):11872–11880, 2012.

[63] Zhikun Cai and Yang Zhang. Hydrophobicity-driven unfolding of Trp-cage encapsulated between graphene sheets. *Colloids and Surfaces B: Biointerfaces*, 168:103–108, 2018.

[64] Srikanth Sastry, Pablo G. Debenedetti, and Frank H. Stillinger. Signatures of distinct dynamical regimes in the energy landscape of a glass-forming liquid. *Nature*, 393(6685):554–557, 1998.

[65] Michael Schulz. Energy landscape, minimum points, and non-Arrhenius behavior of supercooled liquids. *Physical Review B*, 57(18):11319–11333, 1998.

[66] T. Keyes. Dependence of supercooled liquid dynamics on elevation in the energy landscape. *Physical Review E*, 59(3):3207–3211, 1999.

[67] Dennis L. Malandro and Daniel J. Lacks. Volume dependence of potential energy landscapes in glasses. *The Journal of Chemical Physics*, 107(15):5804–5810, 1997.

[68] Dennis L. Malandro and Daniel J. Lacks. Relationships of shear-induced changes in the potential energy landscape to the mechanical properties of ductile glasses. *The Journal of Chemical Physics*, 110(9):4593–4601, 1999.

[69] Ulf Bengtzelius, W. Götze, and A. Sjölander. Dynamics of supercooled liquids and the glass transition. *Journal of Physics C: Solid State Physics*, 17(33):5915–5934, 1984.

[70] W. Götze and L. Sjögren. Relaxation processes in supercooled liquids. *Reports on Progress in Physics*, 55(3):241–376, 1992.

[71] David R. Reichman and Patrick Charbonneau. Mode-coupling theory. *Journal of Statistical Mechanics: Theory and Experiment*, 2005(05):P05013, 2005.

[72] W. Götze and L. Sjögren. The mode coupling theory of structural relaxations. *Transport Theory and Statistical Physics*, 24(6-8):801–853, 1995.

[73] T. R. Kirkpatrick and P. G. Wolynes. Stable and metastable states in mean-field Potts and structural glasses. *Physical Review B*, 36(16):8552–8564, 1987.

[74] Y. Singh, J. P. Stoessel, and P. G. Wolynes. Hard-sphere glass and the density-functional theory of aperiodic crystals. *Physical Review Letters*, 54(10):1059–1062, 1985.

[75] T. V. Ramakrishnan and M. Yussouff. First-principles order-parameter theory of freezing. *Physical Review B*, 19(5):2775–2794, 1979.

[76] M. Yussouff. Generalized structural theory of freezing. *Physical Review B*, 23(11):5871–5879, 1981.

[77] Vassiliy Lubchenko and Peter G. Wolynes. Barrier softening near the onset of nonactivated transport in supercooled liquids: Implications for establishing detailed connection between thermodynamic and kinetic anomalies in supercooled liquids. *The Journal of Chemical Physics*, 119(17):9088–9105, 2003.

[78] J. P. Stoessel and P. G. Wolynes. Linear excitations and the stability of the hard sphere glass. *The Journal of Chemical Physics*, 80(9):4502–4512, 1984.

[79] Jacob D. Stevenson and Peter G. Wolynes. On the surface of glasses. *The Journal of Chemical Physics*, 129(23):234514, 2008.

[80] Anh D. Phan and Kenneth S. Schweizer. Elastically collective nonlinear Langevin equation theory of glass-forming liquids: Transient localization, thermodynamic mapping, and cooperativity. *The Journal of Physical Chemistry B*, 122(35):8451–8461, 2018.

[81] Anh D. Phan and Kenneth S. Schweizer. Theory of the spatial transfer of interface-nucleated changes of dynamical constraints and its consequences in glass-forming films. *The Journal of Chemical Physics*, 150(4):044508, 2019.

[82] Daniel Diaz-Vela, Jui-Hsiang Hung, and David S. Simmons. Temperature-independent rescaling of the local activation barrier drives free surface nanoconfinement effects on segmental-scale translational dynamics near T_g. *ACS Macro Letters*, 7(11):1295–1301, 2018.

[83] W. Klement Jun, R. H. Willens, and Pol Duwez. Non-crystalline structure in solidified gold-silicon alloys. *Nature*, 187(4740):869–870, 1960.

[84] H. Liebermann and C. Graham. Production of amorphous alloy ribbons and effects of apparatus parameters on ribbon dimensions. *IEEE Transactions on Magnetics*, 12(6):921–923, 1976.

[85] Ratnamala Roy and A. K. Majumdar. Thermomagnetic and transport properties of metglas 2605 SC and 2605. *Journal of Magnetism and Magnetic Materials*, 25(1):83–89, 1981.

[86] V. Ponnambalam, S. Joseph Poon, and Gary J. Shiflet. Fe-based bulk metallic glasses with diameter thickness larger than one centimeter. *Journal of Materials Research*, 19(5):1320–1323, 2004.

[87] W. H. Wang, C. Dong, and C. H. Shek. Bulk metallic glasses. *Materials Science and Engineering: R: Reports*, 44(2–3):45–89, 2004.

[88] Jan Schroers. Processing of bulk metallic glass. *Advanced Materials*, 22(14):1566–1597, 2010.

[89] Golden Kumar, Amish Desai, and Jan Schroers. Bulk metallic glass: The smaller the better. *Advanced materials*, 23(4):461–476, 2011.

[90] Alan Russell and Kok Loong Lee. *Structure-property relations in nonferrous metals*. John Wiley & Sons, 2005.

[91] Wei Hua Wang. The elastic properties, elastic models and elastic perspectives of metallic glasses. *Progress in Materials Science*, 57(3):487–656, 2012.

[92] Thierry Gloriant. Microhardness and abrasive wear resistance of metallic glasses and nanostructured composite materials. *Journal of Non-Crystalline Solids*, 316(1):96–103, 2003.

[93] A. I. Salimon, M. F. Ashby, Y. Brechet, and A. L. Greer. Bulk metallic glasses: What are they good for? *Materials Science and Engineering: A*, 375:385–388, 2004.

[94] Yasunory Saotome and H. Iwazaki. Superplastic extrusion of microgear shaft of 10 μm in module. *Microsystem Technologies*, 6(4):126–129, 2000.

[95] Golden Kumar, Hong X. Tang, and Jan Schroers. Nanomoulding with amorphous metals. *Nature*, 457(7231):868–872, 2009.

[96] Pejman Hojati-Talemi, Mark A. Gibson, Daniel East, and George P. Simon. High performance bulk metallic glass/carbon nanotube composite cathodes for electron field emission. *Applied Physics Letters*, 99(19):194104, 2011.

[97] Seok-Woo Lee, Moo-Young Huh, Eric Fleury, and Jae-Chul Lee. Crystallization-induced plasticity of Cu-Zr containing bulk amorphous alloys. *Acta Materialia*, 54(2):349–355, 2006.

[98] Loup Verlet. Computer "experiments" on classical fluids. I. Thermodynamical properties of Lennard-Jones molecules. *Physical Review*, 159(1):98–103, 1967.

[99] Steve Plimpton. Fast parallel algorithms for short-range molecular dynamics. *Journal of Computational Physics*, 117(1):1–19, 1995.

[100] Y. Q. Cheng, E. Ma, and H. W. Sheng. Atomic level structure in multicomponent bulk metallic glass. *Physical Review Letters*, 102(24):245501, 2009.

[101] Shūichi Nosé. A unified formulation of the constant temperature molecular dynamics methods. *The Journal of Chemical Physics*, 81(1):511–519, 1984.

[102] Shūichi Nosé. A molecular dynamics method for simulations in the canonical ensemble. *Molecular Physics*, 52(2):255–268, 1984.

[103] William G. Hoover. Canonical dynamics: Equilibrium phase-space distributions. *Physical Review A*, 31(3):1695–1697, 1985.

[104] Nathan P. Walter, Abhishek Jaiswal, Zhikun Cai, and Yang Zhang. Liquidlib: A comprehensive toolbox for analyzing classical and ab initio molecular dynamics simulations of liquids and liquid-like matter with applications to neutron scattering experiments. *Computer Physics Communications*, 228:209–218, 2018.

[105] William Humphrey, Andrew Dalke, and Klaus Schulten. VMD: Visual molecular dynamics. *Journal of Molecular Graphics*, 14(1):33–38, 1996.

[106] Jean-Pierre Hansen and Ian R. McDonald. *Theory of simple liquids*. Elsevier, 1990.

[107] Chunguang Tang and Peter Harrowell. Chemical ordering and crystal nucleation at the liquid surface: A comparison of $Cu_{50}Zr_{50}$ and $Ni_{50}Al_{50}$ alloys. *The Journal of Chemical Physics*, 148(4):044509, 2018.

[108] Jean-Pierre Hansen and Ian Ranald McDonald. *Theory of simple liquids: with applications to soft matter*. Academic Press, 2013.

[109] Kirit N. Lad and Arun Pratap. Velocity autocorrelation function for simple liquids and its application to liquid metals and alloys. *Physical Review E*, 70(5):051201, 2004.

[110] Kenneth R. Harris. The fractional Stokes-Einstein equation: Application to Lennard-Jones, molecular, and ionic liquids. *The Journal of Chemical Physics*, 131(5):054503, 2009.

[111] J. F. Douglas and Dino Leporini. Obstruction model of the fractional Stokes-Einstein relation in glass-forming liquids. *Journal of Non-Crystalline Solids*, 235:137–141, 1998.

[112] Kenneth S. Schweizer and Erica J. Saltzman. Activated hopping, barrier fluctuations, and heterogeneity in glassy suspensions and liquids. *The Journal of Physical Chemistry B*, 108(51):19729–19741, 2004.

[113] YounJoon Jung, Juan P. Garrahan, and David Chandler. Excitation lines and the breakdown of Stokes-Einstein relations in supercooled liquids. *Physical Review E*, 69(6):061205, 2004.

[114] Albert C. Pan, Juan P. Garrahan, and David Chandler. Heterogeneity and growing length scales in the dynamics of kinetically constrained lattice gases in two dimensions. *Physical Review E*, 72(4):041106, 2005.

[115] Shaopeng Pan, Z. W. Wu, W. H. Wang, M. Z. Li, and Limei Xu. Structural origin of fractional Stokes-Einstein relation in glass-forming liquids. *Scientific Reports*, 7:39938, 2017.

[116] Ryogo Kubo. Statistical-mechanical theory of irreversible processes. I. General theory and simple applications to magnetic and conduction problems. *Journal of the Physical Society of Japan*, 12(6):570–586, 1957.

[117] Giulio Biroli and J.-P. Bouchaud. Diverging length scale and upper critical dimension in the Mode-Coupling Theory of the glass transition. *Europhysics Letters*, 67(1):21, 2004.

[118] M. Scott Shell, Pablo G. Debenedetti, and Frank H. Stillinger. Dynamic heterogeneity and non-Gaussian behaviour in a model supercooled liquid. *Journal of Physics: Condensed Matter*, 17(49):S4035, 2005.

[119] Bo Wang, James Kuo, Sung Chul Bae, and Steve Granick. When Brownian diffusion is not Gaussian. *Nature Materials*, 11(6):481, 2012.

[120] Lijin Wang, Ning Xu, W. H. Wang, and Pengfei Guan. Revealing the link between structural relaxation and dynamic heterogeneity in glass-forming liquids. *Physical Review Letters*, 120(12):125502, 2018.

[121] Zihan Huang, Gaoming Wang, and Zhao Yu. Non-Gaussian parameter in k-dimensional Euclidean space. *arXiv preprint arXiv:1511.06672*, 2015.

[122] Jörg Behler and Michele Parrinello. Generalized neural-network representation of high-dimensional potential-energy surfaces. *Physical Review Letters*, 98(14):146401, 2007.